IEEE Access
Multidisciplinary | Rapid Review | Open Access Journal

Received June 17, 2020, accepted June 30, 2020, date of publication July 7, 2020, date of current version July 20, 2020.

Digital Object Identifier 10.1109/ACCESS.2020.3007774

Evolution of Netted Radar Systems

ZHE GENG, (Member, IEEE)
College of Electronic and Information Engineering, Nanjing University of Aeronautics and Astronautics, Nanjing 210016, China
e-mail: zhe.geng@ieee.org

This work was supported in part by the China Ministry of Industry and Information Technology Foundation under Grant MJ-2018-S-28, and in part by the Research Funds for New Faculty of NUAA under Grant 1004-YAH19111.

ABSTRACT The netted radar systems are known for being able to provide higher target detection probabilities, more accurate measurements, and better multi-target tracking performance than the monostatic/bistatic radar systems by exploiting information fusion processing. Simple radar networks made of multiple independent monostatic radars with decentralized processing have been around for several decades. In contrast, sophisticated radar networks with centralized data fusion only emerged during the last few years thanks to the development in high-speed digital processing and precise time/phase synchronization. Although the advanced radar networks offer the potential ability to detect stealth targets and low probability of intercept radar signal, there are many technical challenges to be solved before they could evolve from concepts in the research paper to implementable systems in the real-world. By presenting the various target detection and parameter estimation approaches adopted by the distributed MIMO radar, the passive radar network, the hybrid active-passive radar network, and the MIMO synthetic aperture radar (SAR), we lay out the foundation for the future research to be conducted to solve the key issues limiting the practical performance of these advanced radar networks.

INDEX TERMS Multistatic radar, MIMO radar, passive radar, radar network.

I. INTRODUCTION

Netted radar systems consisting of multiple transmitting and receiving facilities that are widely separated have been the subject of a high degree of interest for many years [1]. The evolution of radar networks with increasing levels of sophistication is shown in FIGURE 1 [2], [3]. Simple radar networks composed of independent monostatic radars operating at different frequencies have been around for several decades, which usually employ decentralized data fusion at the track level. For example, in a typical target-tracking scenario, multiple moving target tracks obtained from different incident angles by multiple widely-separated radars could be fused to improve the multi-target tracking performance [4]. The National Weather Service WSR-88D Next-Generation Radar (NEXRAD) used for nationwide weather observation in North America also belongs to this group of simple radar network [5]. Another form of conventional radar network is the multistatic radar made of multiple receivers (RXs) and single transmitter (TX) that could either be co-located with one of the RXs or not (note: the former configuration provides both monostatic and bistatic operation results), where target positioning could be carried out by measuring the time-difference-of-arrival (TDOA) and using the spherical-intersection (SX) method given that the number of RXs is greater than 3 [6]. Target detection and localization with multistatic radar composed of multiple TXs and RXs with decentralized processing at the post-detection level have been detailed in [7]. However, centralized processing at the pre-detection raw data level was only briefly discussed in [7] due to the various technical difficulties involved in practical implementation 20 years ago, such as the limited speed of digital processing, the limited capacity of data transmission lines, the errors in time/phase synchronization, etc. The U.S. has been exploring the possibility of combining separate national radar networks into one multi-function phased array (MPAR) network since 2007 [8]. More recently, both Rockwell Collins, Inc. and Honeywell International Inc. have filed patents on methods to merging the weather data from multiple ground-based NEXRAD radar systems and airborne weather radar systems to provide more accurate weather information to the aircrafts [9]–[11]. By picking the optimum radar waveform "on the fly" from the waveform set (e.g. via adaptive pulse compression [12]), the airborne weather radar systems could be upgraded to support multi-mission (weather observation, sense-and-avoid, imaging) [13], [14]. Hence it is

The associate editor coordinating the review of this manuscript and approving it for publication was Chengpeng Hao.

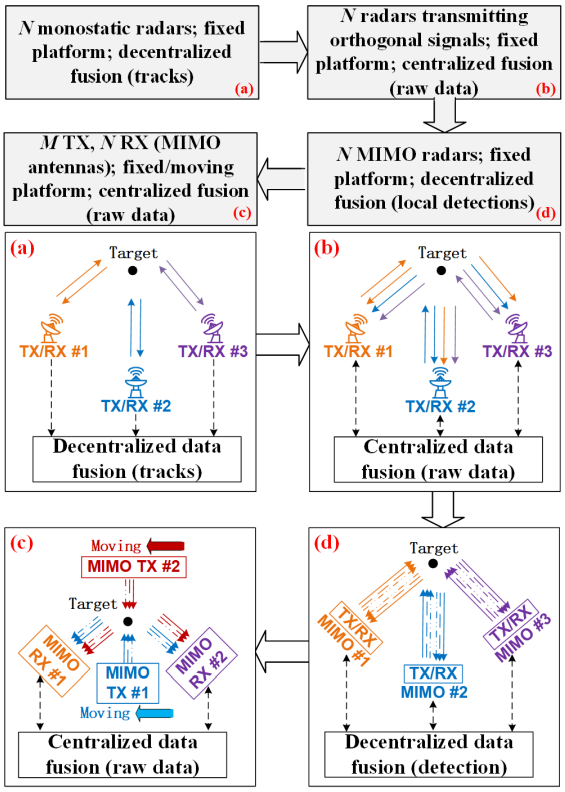

FIGURE 1. Evolution of radar networks. (a) Conventional radar network composed of simple monostatic radars with decentralized processing. (b) Distributed MIMO radar with centralized data fusion. (c) The hybrid coherent/distributed MIMO radar made of ground-based co-located MIMO radars. (d) The hybrid coherent/distributed MIMO radar as a mixture of ground-based and airborne TX/RX nodes equipped with MIMO antennas.

reasonable to predict that a more sophisticated and powerful air-ground netted radar system is around the corner.

A. ORTHOGONAL NETTED RADAR SYSTEMS

With the recent technology advancement in high-speed digital processing and precise time/phase synchronization, advanced radar networks with RXs that are capable of processing the reflected signals associated with the probing signals from all the TXs (i.e. cooperative signal reception) become technically feasible [1]. The orthogonal netted radar systems (ONRS) proposed in [15] consists of N pulse radar stations with co-located TX-RX, and the signals transmitted from different TXs are orthogonal to each other. Each RX in the ONRS is equipped with N parallel matched filters, so that the reflected signals associated with the illuminations from different TXs could be separated and extracted for further processing. For simple radar networks, each RX can only receive and process the reflected signals associated with the probing signals from a specific TX, hence the number of independent echoes from the same target is linearly proportional to the number of receivers (N), i.e. O(N) [15]. In comparison, for an ONRS the number of independent echoes from the same target is increased to O(N^2). The ONRS has a series of advantages over the conventional monostatic/bistatic radar, which include 1) *improved detection performance*; 2) *ad-hoc configuration*; 3) *more accurate target measurement*; 4) *simultaneous measurement of target location, velocity, & acceleration rate*; 5) *more effective target identification*; and 6) *enhanced capabilities in countering sophisticated anti-radar techniques* [15].

B. MIMO RADAR

Although the concept of MIMO radar is relatively new (it was introduced in [16] in 2004), it could be regarded as part of a continuum of different types of netted radar systems instead of a separate subject [2], [3], [15]. MIMO radar systems could be classified as two types: coherent/co-located MIMO radar composed of closely spaced transmit/receive antenna elements and statistical/distributed MIMO radar employing widely separated transmit/receive antennas [17], [18]. Although co-located MIMO radar may be regarded as a special form of netted radar system with each transmit/receive station shrinking into a MIMO antenna element [15], in this work we focus on the distributed MIMO radar (DMR), which observes the same aspect of a target from different angles. The DMR is different from conventional multistatic radar appeared in early literatures in the sense that the reflected signals associated with illuminations from different transmit antennas could be identified and separated at each receiving antenna so that centralized processing could be implemented. Hence the ONRS proposed in [15] could be regarded as an embodiment of the DMR. Compared with monostatic radar, the DMR provides better detection performance against fluctuating target [19], tailored coverage area [20], more accurate target position and velocity estimation [21], [22], richer signal information [23], and increased reliability [23]. A more sophisticated type of DMR is the hybrid co-located/distributed radar network presented in [1], [24]–[27]. In [25], [26], a hybrid radar network composed of one monostatic coherent MIMO radar, one bistatic coherent MIMO radar, and two bistatic phased-array radars was formulated by exploiting the MIMO and phased-array antenna arrays mounted on four airborne moving platforms. In [27], an airborne hybrid co-located/distributed MIMO radar network consisting of multiple transmit and receive MIMO antenna arrays mounted on widely separated moving platforms was considered. Interested readers are referred to these works for more details.

C. PASSIVE RADAR NETWORK (PRN)

Passive radar could be used as a supplement to the active radar since 1) it doesn't require dedicated transmitter or spectrum allocation; 2) it offers superior detection performance against the stealth targets and is immune to the antiradiation missiles (ARMs). Potential candidates for illuminators of opportunity (IOs) include analogue communications systems (e.g. FM [28], [29] & analogue terrestrial TV [30]), digital communications systems (e.g. Wi-Fi [31], [32], digital video broadcasting-terrestrial (DVB-T) [33]–[35], & mobile phones base stations [36], [37]), satellite-borne illuminators

(e.g. Global Navigation Satellite System (GNSS) [38] & Satellite TV (DVB-S) [39]), and terrestrial positioning systems (e.g. [40], [41]). Since the signals transmitted from the IO are generally not known *a priori*, the passive radar receiver is usually equipped with a dedicated reference channel (RC) to collect the direct-path signal from the IO as a reference of the transmitted signal [42]. With the advancement in MIMO radar technology, there has been a steadily increasing interest in developing PRN with widely separated IOs and RXs [36], [37], [43]–[49].

D. HYBRID ACTIVE-PASSIVE RADAR NETWORK (APRN)

The APRN is defined in this work as a radar system that exploits both the dedicated radar transmit waveforms and signals from the IOs. It usually offers better target detection performance than the PRN due to the increased level of control over the sensor geometry and the more flexible transmit waveform design. In [50], it was proposed that an active fallback component (AFC) transmitting low-probability-of-intercept (LPI) signals could be used in conjunction with the passive bistatic radar (PBR), which is capable of operating as a fallback in case the IOs are destroyed in a conflict situation. In [31], [51], [52], APRNs composed of the frequency-modulated continuous wave (FMCW) radar and the WiFi-based passive radar have been considered for short range monitoring. In [53], an APRN consisting of a monostatic coherent MIMO radar and several IOs was proposed, with the TX and the RX assumed to be co-located. Another example of APRN is the deployable multiband passive/active radar (DMPAR) proposed for air surveillance and air defense in [54]–[56], which employs decentralized data fusion processing. Joint radar-communications (JRC) system may be considered as a special form of APRN, which generally offers better performance than the PRN but worse than the active DMR [57]–[65].

E. MULTISTATIC SAR AND MIMO SAR

Synthetic aperture radar (SAR) synthesizes a large phased array antenna aperture by moving an individual antenna array element or the conventional antenna through multiple successive locations in space [66]. Multistatic SAR offers higher mapping rate than the monostatic SAR and could be classified as two types: fully active system and semi-active system [67], [68]. In fully active system, multiple sensors are employed and each sensor has both transmit and receive capabilities, e.g. [69]. In semi-active system, only one sensor is transmitting, and multiple widely distributed sensors are employed to receive the echoes from different angles, e.g. [70]. Fully active multistatic SAR has higher sensitivity and flexibility than the semi-active system at the price of higher computational complexity. The term ''MIMO SAR'' formally appeared in literatures for the first time in 2007 [71]–[74], although the first suggestion of using a MIMO SAR architecture emerged in May 2006 [75]. The MIMO SAR system employs multiple sensors that are simultaneously transmitting and receiving. By exploiting the orthogonality between transmit waveforms, each receiving sensor is able to distinguish the echoes associated with different transmit waveforms. The MIMO SAR could be classified as the coherent MIMO SAR [74], [76] and the distributed MIMO SAR [77], with the latter being our main focus.

F. CONTRIBUTIONS OF THIS WORK

In this work, we present various types of netted radar systems, which include the DMR, the PRN, the APRN, and the MIMO SAR. The advantages of these advanced radar networks over the conventional monostatic radar are summarized, while the key technologies and challenges for implementing them are identified. Our major contributions regarding each type of radar network are summarized as below.

- To illustrate the design principle of knowledge-aided (KA) detectors for DMR, we introduce two detectors for target detection in heterogeneous interference and partially homogeneous interference, respectively, which exhibit better performance than the existing detectors.
- High-speed highly-maneuvering target tracking with DMR is considered, and the transmitted waveforms are adaptively selected from a pre-designed waveform library to minimize the mean squared error (MSE) of the target state estimate.
- The problem of sensor geometry optimization for DMR is considered, and the trajectories of the TXs/RXs mounted on the unmanned aerial vehicles (UAV) are optimized for target localization.
- The performance degradation of the existing detectors designed for PRN in the presence of the direct-path interference, the multipath clutter and the interfering targets is evaluated for the first time.
- The problem of sensor geometry optimization in APRN is discussed for the first time.
- The major advantages of MIMO SAR over monostatic and multistatic SAR are highlighted, and the key technical challenges for implementing MIMO SAR are summarized.

The rest of this work is organized as following. Target detection, measurements, and tracking with DMR are considered in Section II. Target detection and parameter estimation with PRN are discussed in Section III, where various types of interferences are taken into consideration. Sensor geometry optimization in APRN is discussed in Section IV. In Section V, the concepts of monostatic SAR, multistatic SAR, and MIMO SAR are reviewed. Finally, some conclusions are drawn in Section VI.

II. TARGET DETECTION, PARAMETER ESTIMATION, AND TRACKING USING DMR

Target detection, parameter estimation, and tracking are the three primary functions of a DMR system. The process of deciding whether or not a target is present is a problem involving statistical hypothesis testing. In a single-target scenario, the target detection problem is usually formulated as a

binary hypothesis testing problem where two hypotheses are made: the *null hypothesis* (target is absent) and the *alternative hypothesis* (target is present). The radar measurements have to be examined to decide which hypothesis is more likely to be true. In a multi-target scenario with M targets, the target detection problem could be formulated as an M-ary hypothesis testing problem [78]. General statistical signal detection theory could be found in [79], where the commonly used detectors such as the Neyman-Pearson (NP) detector and the generalized likelihood ratio test (GLRT) detector are introduced. Estimators for radar applications are classified as range estimator, Doppler estimator and angle estimator. The lower bound on the variance of any unbiased estimator is set by the Cramer-Rao lower bound (CRLB). A general introduction to widely used estimators such as the maximum likelihood estimator and the best linear unbiased estimator (BLUE) is given in [80]. The estimation accuracy of the target position could be improved by collecting a series of estimates over a period of time and combining them with reasonable assumptions about the target's trajectory, i.e. tracking. Basic tracking theory such as sequential least-squares estimation (LSE) is covered in [80].

Assuming that the readers possess the basic knowledge about the detectors and estimators commonly used by the conventional monostatic radar, in the following we mainly focus on the key technologies and the major challenges corresponding to target detection with DMR. Specifically, the problem of interference suppression, adaptive waveform design for target tracking, and the various approaches to sensor geometry optimization are discussed in Sec. II-A, Sec. II-B, and Sec. II-C, respectively.

A. INTERFERENCE SUPPRESSION

DMR employs large aperture arrays made of widely separated transmit and receive antennas. The transmit waveforms from different antennas are designed to be orthogonal to each other, so that they could be identified and separated at each receive antenna. By exploiting the spatial diversity of the target's radar cross section (RCS), the problem of target fluctuation could be solved. Since different transmit-receive antenna pairs observe clutter scatterers from different transmitter-clutter-receiver paths, the clutter power usually varies significantly from one resolution cell to another and is different for each transmit-receive pair, i.e. nonhomogeneous clutter [19]. The most commonly used clutter models for DMR include the Spherically Invariant Random Vector (SIRV) model [81], the sparse representation model [19], the autoregressive (AR) model [82], the random matrices model [83], and the general model exploiting the persymmetric structure of the interference covariance [84]–[86]. For ground-based stationary DMR, the clutter is near-stationary or slowly moving most of the time. Hence the low-rank sparsity-based clutter model with known clutter subspace [19] or the low-order AR model with known model order [82] could be used to model the clutter for ground-based stationary DMR. In contrast, for airborne DMR, the clutter subspace and the AR model order

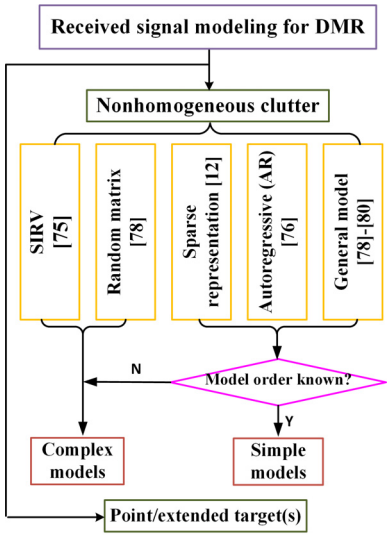

FIGURE 2. Signal models commonly used for the received signal of the DMR. N and Y represent "no" and "yes", respectively.

have to be estimated from the measurement data adaptively [20]. The tree diagram for the commonly used signal models for DMR is shown in FIGURE 2.

Depending on whether the clutter covariance for each transmit-receive antenna pair shares the same covariance structure, the clutter for DMR could be classified as partially homogeneous clutter and heterogeneous clutter. The partially homogeneous clutter may be represented by the compound Gaussian model with distinct texture term, which is a positive random variable accounting for the clutter power, and common covariance structure, which is a random matrix following the inverse complex Wishart distribution, for each transmit-receive pair [87]. The heterogeneous clutter may be modeled as i.i.d. complex zero-mean Gaussian vectors with random covariance matrices, and the different clutter power levels for each transmit-receive pair may be represented by unknown deterministic scaling factors [83].

The most challenging issue in clutter suppression for DMR is the lack of i.i.d. training data in nonhomogeneous clutter environment. Specifically, for DMR consisting of M transmit antennas and N receive antennas, at least $2KMN$ i.i.d. training data samples free of target signal components are required to achieve a SINR loss of 3dB if the conventional sample covariance matrix (SCM) based clutter suppression method is to be used, where K is the number of pulses transmitted from each antenna per CPI. Many researchers believe that so-called knowledge-aided (KA) covariance estimation is a possible solution to alleviating the requirement on training data, and a series of training-free and low-sample-support KA detectors have been designed by exploiting the prior knowledge of the clutter that might be available [83], [88].

In the following, we introduce two detectors for target detection in heterogeneous interference and partially homogeneous interference, respectively. To address heterogeneous interference, the local interference power in the cell under

test, $u_{m,n,0}$, is supposed to be an unknown deterministic number, and the interference covariance is assumed to be a random matrix. A detector termed as the general knowledge-aided (GKA) detector is designed by incorporating the prior knowledge about the interference into the geometric approach proposed in [86]. For partially homogeneous interference, $u_{m,n,0}$ is assumed to be a random variable following a specific pdf, such as K-distribution, student-t distribution, or Weibull distribution. The texture-specific clairvoyant (TCL) detectors corresponding to various pdfs are first obtained assuming known interference covariance. After that, the interference covariance is estimated by jointly exploiting the sample covariance matrix (SCM), the persymmetric structure of $\Sigma_{m,n}$, and the prior knowledge matrix. Since the weighting factor is adaptively selected based on convex combination, this detector is termed as the texture-specific persymmetric convex combination (TPCC) detector. The design process of the GKA detector and the TPCC detector are detailed below.

1) HETEROGENEOUS INTERFERENCE

The interference signal $\mathbf{c}_{m,n,l}$ ($m = 1, \ldots, M; n = 1, \ldots, N; l = 0, 1, \ldots, L$) is modeled as

$$\mathbf{c}_{m,n,l} = \sqrt{u_{m,n,l}}\mathbf{g}_{m,n,l}, \tag{1}$$

where $u_{m,n,l}$ is a positive unknown deterministic number controlling the local scattering power [83] and $\mathbf{g}_{m,n,l}$ is a K-dimensional, independent, zero-mean complex Gaussian vector. It is further assumed that

$$\begin{aligned} E\{\mathbf{c}_{m,n,0}\mathbf{c}_{m,n,0}^H | u_{m,n,0}, \boldsymbol{\Sigma}_{m,n}\} &= u_{m,n,0}\boldsymbol{\Sigma}_{m,n}, \\ E\{\mathbf{c}_{m,n,l}\mathbf{c}_{m,n,l}^H | u_{m,n,l}, \boldsymbol{\Xi}_{m,n}\} &= u_{m,n,l}\boldsymbol{\Xi}_{m,n}, \quad l = 1, \ldots, L, \\ \boldsymbol{\Sigma}_{m,n} | \boldsymbol{\Xi}_{m,n} &\sim \mathcal{CW}^{-1}((\zeta_{m,n}-K)\boldsymbol{\Xi}_{m,n}, \zeta_{m,n}). \end{aligned} \tag{2}$$

where $\boldsymbol{\Sigma}_{m,n}$ and $\Xi_{m,n}$ represent the covariance structure of the primary and the secondary training data, respectively, and $\mathcal{CW}^{-1}$ represents the inverse complex Wishart distribution with $\zeta_{m,n} > K$ degrees of freedom. As $\zeta_{m,n}$ increases, the variance of $\boldsymbol{\Sigma}_{m,n}$ decreases. Suppose that $\Xi_{m,n}$ is known and $\Xi_{m,n} = \boldsymbol{\Sigma}_{m,n}$, the clairvoyant GLRT (CL-GLRT) detector is given by

$$\Lambda_{GLRT-CL} = \prod_{m=1}^{M_T}\prod_{n=1}^{N}\left[1 - \frac{\mathbf{s}_{m,n}^H\boldsymbol{\Sigma}_{m,n}^{-1}\mathbf{y}_{m,n,0}}{(\mathbf{s}_{m,n}^H\boldsymbol{\Sigma}_{m,n}^{-1}\mathbf{s}_{m,n})(\mathbf{y}_{m,n,0}^H\boldsymbol{\Sigma}_{m,n}^{-1}\mathbf{y}_{m,n,0})}\right]^{-K} \underset{H_0}{\overset{H_1}{\gtrless}} \xi'. \tag{3}$$

where ξ' is the threshold. By minimizing the Euclidean distance between the primary and the secondary covariance, $\boldsymbol{\Sigma}_{m,n}$ is estimated as [89]

$$\begin{aligned} \check{\mathbf{S}}_{m,n,l} &= \mathbf{U}_{m,n,l}\Lambda_{m,n,l}\mathbf{U}_{m,n,l}^H, \\ \Lambda_{m,n,l} &= \mathrm{diag}([\varepsilon_{m,n}\lambda_{m,n,l}, \lambda_{m,n,l}, \ldots, \lambda_{m,n,l}]), \\ \lambda_{m,n,l} &= \max\left(1, \frac{||\check{\mathbf{c}}_{m,n,l}||^2\varepsilon_{m,n}}{\varepsilon_{m,n}^2 + K - 1}\right) \end{aligned} \tag{4}$$

where $\check{\mathbf{c}}_{m,n,l} = \mathbf{c}_{m,n,l}/\bar{\sigma}_{m,n,I}^2$ with $\bar{\sigma}_{m,n,I}^2$ being the lower bound to the white interference power, $\mathbf{U}_{m,n,l}$ is a unitary matrix of the eigenvectors of $\check{\mathbf{c}}_{m,n,l}\check{\mathbf{c}}_{m,n,l}^H$ with the 1st eigenvector corresponding to the eigenvalue $\left\|\check{\mathbf{c}}_{m,n,l}\right\|^2$, and $\varepsilon_{m,n} > 1$ is the upper bound to the condition number of the covariance [90], [91]. Based on the numerical simulations, the covariance estimate in (4) is only accurate when $\boldsymbol{\Xi}_{m,n} = \boldsymbol{\Sigma}_{m,n}$, i.e. the interference is partially homogeneous. To improve the estimation accuracy in heterogeneous interference, we resort to the prior knowledge matrix $\hat{\boldsymbol{\Sigma}}_{m,n,P} = \boldsymbol{\Sigma}_{m,n} \odot (\mathbf{t}_{m,n}\mathbf{t}_{m,n}^H)$, where $\odot$ denotes the Hadamard product and $\mathbf{t}_{m,n}$ is a vector of i.i.d. Gaussian random variables with mean of 1 and variance of $\sigma_{m,n,\mathrm{KA}}^2$. The smaller $\sigma_{m,n,\mathrm{KA}}^2$ is, the more precise the prior knowledge is. The general linear combination (GLC) method is used to minimize the mean-squared error (MSE), and the weighting factors $\varpi_{m,n}$ and $\eta_{m,n}$ are selected adaptively by solving the optimization problem [92]

$$\begin{aligned} &\min_{\varpi_{m,n},\eta_{m,n}} E\{||\widehat{\boldsymbol{\Sigma}}_{m,n,G} - \boldsymbol{\Sigma}_{m,n}||^2\}, \\ &\text{s.t. } \widehat{\boldsymbol{\Sigma}}_{m,n,G} = \varpi_{m,n}\widehat{\boldsymbol{\Sigma}}_{m,n,P} + \eta_{m,n}\widehat{\boldsymbol{\Xi}}_{m,n,S}. \end{aligned} \tag{5}$$

To illustrate the advantage of the GKA detector over the existing detectors, a 2×2 DMR is considered in the following for the numerical performance evaluations without losing generality. A far-field point is assumed to be located at the origin. The two transmitters are assumed to be located at (6.0, −7.0) km and (−6.7, 2.8) km, respectively. The two receivers are assumed to be located at (−9.0, −4.9) km and (4.6, 5.8) km, respectively. The target is moving at 15 m/s, the moving direction of the target is randomly selected from [−180°, 180°] in each Monte Carlo (MC) trial, and the bistatic Doppler of the target changes from run to run. It is further assumed that $K = 8$ pulses are transmitted per CPI, the PRF is 500 Hz, the carrier frequency is 1 GHz, and $L = 10$. A fluctuating target is considered. The complex target amplitude $\alpha_{m,n}$ changes from trial to trial and is assumed to follow a complex Gaussian distribution with zero mean and unit variance. It is further assumed that the interference power is 20 dB, $\zeta_{m,n} = 30$, and $\sigma_{m,n,KA}^2 = 0.1$. The detection probabilities of the GKA detector in heterogenous interference with inverse Gamma distributed texture are plotted in FIGURE 3 assuming SINR = 10 dB. The shape parameter and the scale parameter are set as $\beta_{m,n} = \rho_{m,n} - 1 = 4$, so that $E\{u_{m,n,0}\} = 1$. For SCM-GLRT, the interference covariance is estimated from

$$\hat{\boldsymbol{\Sigma}}_{m,n,,S} = \frac{1}{L}\sum\nolimits_{l=1}^{L}\mathbf{y}_{m,n,l}\mathbf{y}_{m,n,l}^H \tag{6}$$

It could be seen from FIGURE 3 that although the performance of the GKA detector is slightly inferior to that of the CL-GLRT detector, which is the clairvoyant detector serving as the performance upper bound of all the detectors, the GKA detector exhibits much better performance than the conventional SCM-GLRT. Moreover, compared with the Euclidean detector proposed in [89], which doesn't utilize any prior

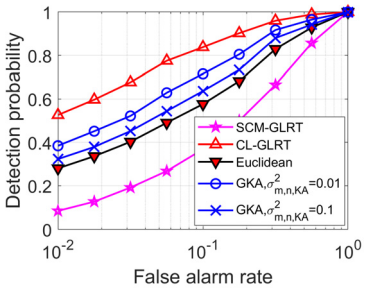

FIGURE 3. Detection performances of the GKA detector in heterogeneous interferences for various P_{fa}. Although the performance of the GKA detector is slightly inferior to that of the CL-GLRT detector, which is the clairvoyant detector serving as the performance upper bound of all the detectors, the GKA detector exhibits better performance than non-KA detectors such as the Euclidean detector proposed in [92] and the conventional SCM-GLRT.

knowledge regarding the interference covariance structure, the GKA detector provides higher detection probabilities even in the case that the prior knowledge is not very accurate, i.e. $\sigma^2_{m,n,\mathrm{KA}} = 0.1$.

2) PARTIALLY HOMOGENEOUS INTERFERENCE

For partially homogeneous interference with $u_{m,n,0}$ following a specific pdf, the optimum detector is no longer the CL-GLRT detector given in (3). Assume that the interferences in the primary and the secondary data associated with the same TX-RX pair share the same covariance matrix structure but have different power levels. It follows that

$$E\{\mathbf{c}_{m,n,0}\mathbf{c}^H_{m,n,0}|u_{m,n,0}, \boldsymbol{\Sigma}_{m,n}\} = E\left\{u_{m,n,0}\right\}\boldsymbol{\Sigma}_{m,n}, . \quad (7)$$

Without loss of generality, we assume that $E\{u_{m,n,l}\} = 1$ [87]. $\boldsymbol{\Sigma}_{m,n}$ is modeled as inverse complex Wishart distributed random matrices with degrees of freedom as $\mu_{m,n}$, i.e.

$$\boldsymbol{\Sigma}_{m,n} \sim \mathcal{CW}^{-1}((\mu_{m,n} - K)\hat{\boldsymbol{\Sigma}}_{m,n}, \mu_{m,n}). \quad (8)$$

where $\hat{\boldsymbol{\Sigma}}_{m,n}$ is the mean of $\boldsymbol{\Sigma}_{m,n}$. In this case, the general form of the GLRT detector using only the primary data is

$$\frac{\max\limits_{\boldsymbol{\alpha}} \prod_{m,n} \int_0^{+\infty} u_{m,n,0}^{-K} \exp\{-p_{m,n,0}/u_{m,n,0}\} f(u_{m,n,0}) du_{m,n,0}}{\prod_{m,n} \int_0^{+\infty} u_{m,n,0}^{-K} \exp\{-q_{m,n,0}/u_{m,n,0}\} f(u_{m,n,0}) du_{m,n,0}} \underset{H_0}{\overset{H_1}{\gtrless}} \xi,$$

$$p_{m,n,0} = (\mathbf{y}_{m,n,0} - \alpha_{m,n}\mathbf{s}_{m,n})^H \boldsymbol{\Sigma}^{-1}_{m,n}(\mathbf{y}_{m,n,0} - \alpha_{m,n}\mathbf{s}_{m,n}),$$
$$q_{m,n,0} = \mathbf{y}^H_{m,n,0}\boldsymbol{\Sigma}^{-1}_{m,n}\mathbf{y}_{m,n,0}. \quad (9)$$

Suppose that $u_{m,n,0}$ follows the inverse Gamma distribution with the shape parameter $\rho_{m,n} > 2$ and the scale parameter $\beta_{m,n} > 0$, the pdf of $u_{m,n,0}$ is

$$f_{IG}(\lambda_{m,n,0}) = \frac{\beta_{m,n}^{\rho_{m,n}} \lambda_{m,n,0}^{-(\rho_{m,n}+1)}}{\Gamma(\rho_{m,n})} \exp\left(-\beta_{m,n}/\lambda_{m,n,0}\right) \quad (10)$$

and the amplitude pdf of the interference follows the student-t distribution [93]. Plugging (10) into (9), the TCL detector for compound Gaussian interference with inverse Gamma distributed texture (TCL-IG) is obtained as

$$\begin{aligned}\Lambda_{TCL-IG1} &= \prod_{mn} \frac{q_{m,n,0} - p_{m,n,0}}{\beta_{m,n} + q_{m,n,0}} \\ &= \prod_{mn} \Lambda_{m,n,0}(\mathbf{y}_{m,n,0}) \frac{\mathbf{y}^H_{m,n,0}\boldsymbol{\Sigma}^{-1}_{m,n}\mathbf{y}_{m,n,0}}{\beta_{m,n} + \mathbf{y}^H_{m,n,0}\boldsymbol{\Sigma}^{-1}_{m,n}\mathbf{y}_{m,n,0}} \\ &\underset{H_0}{\overset{H_1}{\gtrless}} \xi_{TCL-IG1}, \end{aligned} \quad (11)$$

where $\Lambda_{m,n,0}(\mathbf{y}_{m,n,0})$ is the normalized matched filter (NMF) given by

$$\Lambda_{m,n,0}(\mathbf{y}_{m,n,0}) = \frac{\mathbf{s}^H_{m,n}\boldsymbol{\Sigma}^{-1}_{m,n}\mathbf{y}_{m,n,0}}{(\mathbf{s}^H_{m,n}\boldsymbol{\Sigma}^{-1}_{m,n}\mathbf{s}_{m,n})(\mathbf{y}^H_{m,n,0}\boldsymbol{\Sigma}^{-1}_{m,n}\mathbf{y}_{m,n,0})}. \quad (12)$$

Since the detection threshold associated with (11) is much less than 1 for $M > 1$, $N > 1$, the TCL-IG detector is implemented in numerical simulations as

$$\Lambda_{TCL-IG} = \prod_{mn} [1 - \Lambda_{TLS-IG1}]^{-K} \underset{H_0}{\overset{H_1}{\gtrless}} \xi_{TLS-IG}, \quad (13)$$

where ξ_{TLS-IG} is the detection threshold. The final covariance estimate $\hat{\boldsymbol{\Sigma}}_{m,n,T}$ could be obtained by jointly exploiting the sample covariance matrix (SCM), the persymmetric structure of $\boldsymbol{\Sigma}_{m,n}$, and the prior knowledge matrix $\hat{\boldsymbol{\Sigma}}_{m,n,KA} = \hat{\boldsymbol{\Sigma}}_{m,n} \odot (\mathbf{t}_{m,n}\mathbf{t}^H_{m,n})$ using the persymmetric convex combination (PCC) method proposed in [95]. Finally, the TPCC-IG detector is obtained by plugging the covariance estimate $\hat{\boldsymbol{\Sigma}}_{m,n,T}$ into (13).

The detection probabilities of the TCL-IG detector, the TPCC-IG detector, the PCC-GLRT [95] (i.e. the detector obtained by plugging $\hat{\boldsymbol{\Sigma}}_{m,n,T}$ into (3)), the KA-P-GLRT [96], the SCM-GLRT, and the CL-GLRT in partially homogeneous interference with $u_{m,n,0}$ following the inverse Gamma distribution ($\beta_{m,n} = \rho_{m,n} - 1 = 9$, $\mu_{m,n} = 30$) are plotted in FIGURE 4 assuming SINR = 10 dB. The parameters of the DMR used to generate these figures are the same with the ones used to generate FIGURE 3. Among these detectors, the TCL-IG detector and the CL-GLRT are clairvoyant detectors assuming known $\boldsymbol{\Sigma}_{m,n}$, with the former exhibiting better performance. The reason behind this is that the CL-GLRT was derived assuming that $u_{m,n,0}$ is an unknown deterministic number that could take on any value with equal probability, which is equivalent to ignoring the *a priori* knowledge regarding the pdf of $u_{m,n,0}$. Similarly, the TPCC-IG detector is shown to outperform the PCC-GLRT [95] and the KA-P-GLRT [96], which also jointly exploit the SCM, the persymmetric structure of $\boldsymbol{\Sigma}_{m,n}$, and the prior knowledge matrix.

It is worth pointing out that, despite of the promising preliminary simulation results presented above, the full potential of two KA detectors introduced in this section and their limitations need to be validated with a more comprehensive analysis, which is beyond the scope of this work. Moreover,

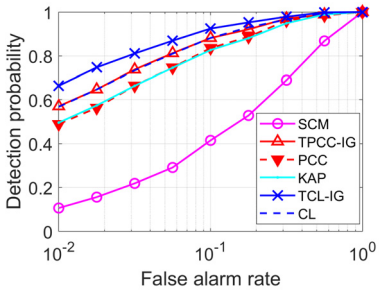

FIGURE 4. Detection performances of the TPCC-IG detector in partially homogeneous interferences for various P_{fa}. It could be seen that for clairvoyant detectors, the TCL-IG have better performance than the CL-GLRT, which was derived assuming that $u_{m,n,0}$ could take on any value with equal probability. Moreover, the proposed TPCC-IG outperform other KA detectors such as the PCC and the KAP.

although the prior knowledge regarding the clutter covariance structure could be exploited to compensate for the lack of i.i.d. training data in heterogenous clutter for ground-based stationary DMR, it was pointed out in [97] that the clutter covariance structure has to be estimated from the measurement data adaptively when DMR carried by airborne platforms is concerned. And it was also shown in the simulation results of [97] that the low-rank sparsity-based clutter suppression method proposed in [20] exhibits a performance degradation when testing against more realistic, more complicated clutter models. In a word, how to effectively suppress the nonhomogeneous clutter encountered by the DMR remains a challenging technical problem that needs to be solved to realize the full potential of the DMR.

B. WAVEFORM DESIGN

The performance of DMR, such as the range/Doppler resolution, the target parameter measurement accuracy, and the capability to suppress interferences, depends highly on the waveform properties of the signals transmitted by each TX. For target tracking with DMR, the ability of each TX to adjust its probing signals adaptively in real-time would lead to higher target localization accuracy [98]–[100]. It is worth pointing out that the optimum solution to the adaptive waveform design problem depends on many factors, which includes the kinematic state of the target, the relative position of the target and radar, the interference-to-noise ratio of the echo signals received by each RX, and the data fusion mechanism, i.e. centralized/decentralized processing. In [101], target tracking using cognitive radar system composed of multiple radars mounted on UAVs is considered, and the expected cross-entropy is used as the objective function. Three key techniques are incorporated in the proposed cognitive radar system: waveform design, path planning, and sensor selection. It should be noted that the waveform library in [101] is very limited, which only includes three different modulated frequencies. In [102], joint transmitter waveform and receiver path optimization is considered, where the waveform is adaptively selected from a waveform library consisting of multiple Gaussian linear frequency modulated (LFM) waveforms with various parameters. The waveform selection method is later extended to the interacting multiple model (IMM) in [103], which is briefly reviewed in the following.

It is assumed that the target motion is governed by the kinematic model $\mathbf{x}_{k+1} = \mathbf{F}\mathbf{x}_k + \mathbf{w}_k$, where $\mathbf{x}_k$ is the target kinematic state vector at discrete-time instant k, $\mathbf{F}$ is the state transition matrix, and $\mathbf{w}_k$ is the process noise modeled as independent Gaussian-distributed variable with zero-mean and covariance $\mathbf{Q}$. Suppose that the target is moving with near constant velocity and the state vector is given by $\mathbf{x}_k = [\mathbf{p}_k^T, \mathbf{v}_k^T]^T$, where $\mathbf{p}_k$ and $\mathbf{v}_k$ are the position and the velocity of the target at time instant $k \in \{0, 1, 2, \ldots\}$, respectively. According to [103], the transition matrix and the covariance matrix of the process noise are, respectively,

$$\mathbf{F} = \begin{bmatrix} \mathbf{I}_{2\times 2} & T\mathbf{I}_{2\times 2} \\ \mathbf{0}_{2\times 2} & \mathbf{I}_{2\times 2} \end{bmatrix}, \quad \mathbf{Q} = \begin{bmatrix} \frac{T^3}{3}\mathbf{Q}_0 & \frac{T^2}{2}\mathbf{Q}_0 \\ \frac{T^2}{2}\mathbf{Q}_0 & T\mathbf{Q}_0 \end{bmatrix}, \quad (14)$$

where $\mathbf{I}$ and $\mathbf{0}$ are the identity matrix and the zero matrix, respectively, T is the sampling interval, $\mathbf{Q}_0 = diag(q_x, q_y)$, with q_x and q_y representing the power spectral densities of the process noise in x-axis and y-axis, respectively. Note that although the noise covariance matrix given in some recently published paper doesn't match (14), e.g. (12) in [101], we believe that (14) is valid and will follow it in this work. The IMM algorithm treats the motion of the maneuvering target as multiple switching models expressed as $\mathbf{x}_{k+1} = \mathbf{F}(m_{k+1})\mathbf{x}_k + \mathbf{w}_k(m_{k+1})$, where $m_{k+1}\{1, \ldots, M\}$ is a finite-state Markov chain following the transition probabilities of switching from model l to model m, and $\mathbf{w}_k(m_{k+1})$ is the process noise, whose covariance is $E\{\mathbf{w}_k(m_{k+1} = l)\mathbf{w}_k^T(m_{k+1} = l)\} = \mathbf{Q}(m_{k+1} = l)$. The tracking performance is usually evaluated by the state estimation error covariance matrix, which is dependent on the parameters of the transmitted waveform. Specifically, the measurement covariance matrix $\mathbf{P}_{m,k+1|k+1}(\boldsymbol{\psi}_{k+1})$ is a function of the transmitted waveform parameter vector $\boldsymbol{\psi}_{k+1}$ at discrete-time instant $k+1$. Assume that the error covariance of the filtered state estimate for the m-th extended Kalman filter (EKF) component of the IMM-EKF algorithm at time instant $k+1$ is $\mathbf{P}_{m,k+1|k+1}(\boldsymbol{\psi}_{k+1})$, and the tracking performance is characterized by $\mathbf{P}^{\diamond}_{k+1|k+1}(\boldsymbol{\psi})$, which is the combination of the state estimates' error covariance matrices $\mathbf{P}_{1,k+1|k+1}, \mathbf{P}_{2,k+1|k+1}, \ldots, \mathbf{P}_{M,k+1|k+1}$. The waveform optimization problem is formulated as [103]

$$\boldsymbol{\psi}_{k+1}^{opt} = \arg\min_{\boldsymbol{\psi}\in\boldsymbol{\Psi}}\{\text{trace}(\mathbf{P}^{\diamond}_{k+1|k+1}(\boldsymbol{\psi}))\}, \quad (15)$$

where Ψ is the waveform library which may include multiple types of radar waveforms or a single type of radar waveform with various waveform parameters.

In the following we will present an example to illustrate the process of adaptive waveform selection. Consider a DMR composed of one TX and four RXs (see FIGURE 5 (a)). The initial position and velocity of the high-speed highly-maneuvering target are $\mathbf{p}_0 = [25, 0]$ km and $[300, 200]^T$ m/s,

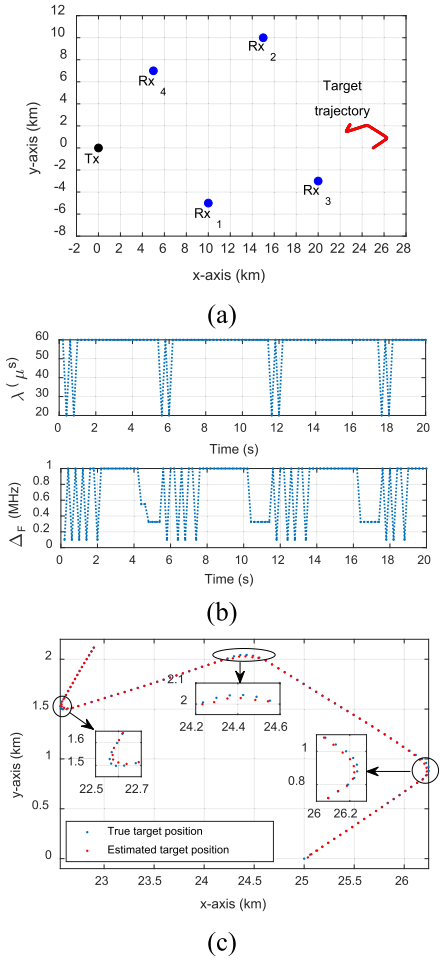

FIGURE 5. Adaptive waveform selection for high-speed highly-maneuvering target tracking. (a) Deployment of the transmitter and four receivers. (b) Waveform selection result. (c) Target trajectory (zoomed-in) and the tracking result.

respectively. The power spectral density of the process noise is $q = q_x = q_y = 10\text{m}^2$. The target starts to change its velocity at $t = 4$ s uniformly until reaches $[-300, 200]^T$ m/s at $t = 5$ s. Then it travels with a nearly constant model again with $q = 10\text{m}^2$. At $t = 10$ s, the target performs another turn and changes its velocity to $[-300, -100]^T$ m/s by $t = 11$ s. Finally, at $t = 16$ s, the target maneuvers again and changes its velocity to $[150, 200]^T$ m/s by $t = 17$ s. Assume that the complex envelope of the LFM waveform is given by [103]

$$\tilde{s}(t) = \left(\frac{1}{\pi\lambda^2}\right)^{\frac{1}{4}} \exp\left(-\left(\frac{1}{2\lambda^2} - j2\pi b\right)t^2\right), \qquad (16)$$

where λ is the Gaussian pulse length parameter and $b = \Delta_f/(2T_s)$ is the frequency modulation rate, with Δ_f and T_s representing the frequency sweep and the effective pulse duration, respectively. The transmitted waveform parameter vector is defined as $\boldsymbol{\psi} = [\lambda, \Delta_f]^T$, and the waveform selection criterion is to minimize the mean squared error (MSE) of the target state estimate, which is equivalent to minimize the trace of the state estimate's error covariance matrix. To realize the optimization goal, the waveform parameters λ and Δ_f are adaptively selected from $\lambda \in [20, 30, 40, 50, 60]$ μs and $\Delta_f \in [0.1, 0.325, 0.55, 0.775, 1]$ MHz, respectively. The waveform selection result is shown in FIGURE 5 (b). The changes of Δ_f at $t = [4, 10, 16]$ sec, i.e., the time instants when the target changes its velocity, are clearly visible. The true target trajectory (zoomed-in) are the estimated target positions are shown in FIGURE 5 (c). It could be seen that even at the target "turning-points", the tracking errors are still small enough to be tolerable.

C. SENSOR GEOMETRY OPTIMIZATION

Since DMR employs multiple widely separated transmitting and receiving facilities, their relative positions to the targets of interest and the observation angles have a huge influence over the target detection, localization and velocity estimation performance of the DMR.

1) TARGET DETECTION

In [105], [106], the positions of antennas are optimized to increase the coverage ratio of the radar system. As an extension of [105], [106], the monitoring requirements are assumed to be changing in [107], and the antennas are dynamically deployed to maximize the coverage ratio. In [108], the positions of DMR sensors are optimized to maximize the SNR. Meanwhile, the goals of antenna position optimization in [109] and [110] are to get an even distribution of signal energy and to minimize the interference power density, respectively.

2) TARGET LOCALIZATION AND TRACKING

In [21], the CRLB for target localization accuracy is developed for DMR employing coherent and noncoherent processing. Symmetrically deploying radars around the target is shown to be optimum in the sense of minimizing the CRLB, and the CRLB on the variance of the estimate is reduced by a factor of $MN/2$ by using DMR with optimum deployment geometry compared to the case where a single antenna is used. The geometric dilution of precision (GDOP) metric, which is the square root of the ratio between the variance of the target location estimate and the variance of the time delay estimation error, is used to map the performance of DMR with a specific deployment geometry over the surveillance area. Later, it is reported in [111] that the mean square error of the BLUE for both coherent and noncoherent target localization techniques for DMR could be factored into two terms dependent on the signal characteristics and the sensor locations, respectively. In [112], the optimal geometry of multistatic radar for 2D target localization is analyzed. The area of error ellipse is minimized by maximizing the determinant of the Fisher information matrix (FIM). It is shown that for DMR consisting of single TX and multiple RXs, the optimum angular separation between each RX and the TX is $\pm\pi/3$. In simulations, target localization with DMR consisting of single TX at fixed position and multiple RXs carried by UAVs is considered, and the trajectories of the UAVs are optimized by maximizing the determinant of FIM using the gradient-descent algorithm. In [113], an approach to

efficiently deploy the antennas for the ultrawideband (UWB) MIMO noise radar was proposed to minimize the target localization error.

In the following, we consider a scenario where multiple independent bistatic radar pairs carried by the UAVs are used for target localization. Although usually the time-of-arrival (TOA) measurements from at least three TX-RX are required to pin-point the target, two TX-RX pairs are enough when the target location is known roughly *a priori*. Suppose that N TX-RX pairs are employed, the Fisher information matrix (FIM) for multistatic TOA localization problem is [103]

$$\begin{aligned}\mathbf{\Phi} &= \sum_{i=1}^{N} \frac{1}{\sigma_i^2}(\mathbf{u}_{t,i} + \mathbf{u}_{r,i})(\mathbf{u}_{t,i} + \mathbf{u}_{r,i})^T, \\ \mathbf{u}_{t,i} &= \left[\cos\theta_{t,i} \ \sin\theta_{t,i}\right], \\ \mathbf{u}_{r,i} &= \left[\cos\theta_{r,i} \ \sin\theta_{r,i}\right], \end{aligned} \tag{17}$$

where $\sigma_i^2 = c^2 E\{e_i^2\}$, with c and e_i representing the speed of light and the TOA measurement noise of the i-th TX-RX pair, respectively; $\mathbf{u}_{t,i}$ and $\mathbf{u}_{r,i}$ are the unit vectors pointing from the i-th TX and the i-th RX to the target, respectively; and $\theta_{t,i}$ ($\theta_{r,i}$) ($i = 1, \ldots, N$) are the angles between $\mathbf{u}_{t,i}$ ($\mathbf{u}_{r,i}$) and the positive x-axis. It has been proved in [103] that maximizing the determinant of the FIM is equivalent to

$$\max_{\beta} \left\{ \left(\sum_{i=1}^{N} \frac{1}{\sigma_i^2} \right)^2 - \left(\sum_{i=1}^{N} \frac{\sin(2\beta_i)}{\sigma_i^2} \right)^2 - \left(\sum_{i=1}^{N} \frac{\cos(2\beta_i)}{\sigma_i^2} \right)^2 \right\} \tag{18}$$

where

$$\beta_i = \frac{\theta_{t,i} + \theta_{r,i}}{2}. \tag{19}$$

According to [103], the optimal solutions to the optimization problem in (18) for $N = 2$ are

$$\left|\beta_1^* - \beta_2^*\right| = \pi/2, \tag{20}$$

and the optimal solutions for $N = 3$ are

$$\begin{aligned}\beta_2^* - \beta_1^* &= \pm\frac{tan^{-1}(\sqrt{\zeta}, b^2 - a^2 - 1)}{2}, \\ \beta_3^* - \beta_1^* &= \mp\frac{tan^{-1}(\sqrt{\zeta}, a^2 - b^2 - 1)}{2}, \end{aligned} \tag{21}$$

where

$$a = \left(\frac{\sigma_1}{\sigma_2}\right)^2, \quad b = \left(\frac{\sigma_1}{\sigma_3}\right)^2, \tag{22}$$

$$\zeta = -(a + b + 1)(a - b + 1)(a + b - 1)(a - b - 1). \tag{23}$$

To illustrate the process of UAV trajectory optimization, we consider some simple examples in the following. Assume that the DMR is composed of two independent bistatic pairs mounted on the UAVs, TX_1-RX_1 and TX_2-RX_2, and each TX/RX is required to maintain a minimum distance from the target (20 km for TXs and 10 km for RXs). The target is supposed to be located at $\boldsymbol{p} = [0, 0]^T$ km. Two different cases are considered, where the initial positions of the TXs and RXs are different. The initial and final positions of the UAVs for Case 1 and Case 2 are shown in FIGURE 6 (a) and (b), respectively. It could be seen that the final positions of TX_1- RX_1 and TX_2- RX_2 form a separation angle of approximately 90° in both cases, which match perfectly with the derivation result in (20). Next, we consider the case where the DMR consisting of three TX-RX pairs. Like the previous example, two different configurations are considered, which are illustrated in FIGURE 6 (c) and (d), respectively. It is shown that the separation angles satisfy $\beta_3^* - \beta_2^* \approx 120°$, $\beta_2^* - \beta_1^* \approx 120°$ in FIGURE 6 (c) and $\beta_3^* - \beta_2^* \approx 60°$, $\beta_2^* - \beta_1^* \approx 60°$ in FIGURE 6 (d), which match the result given in (21).

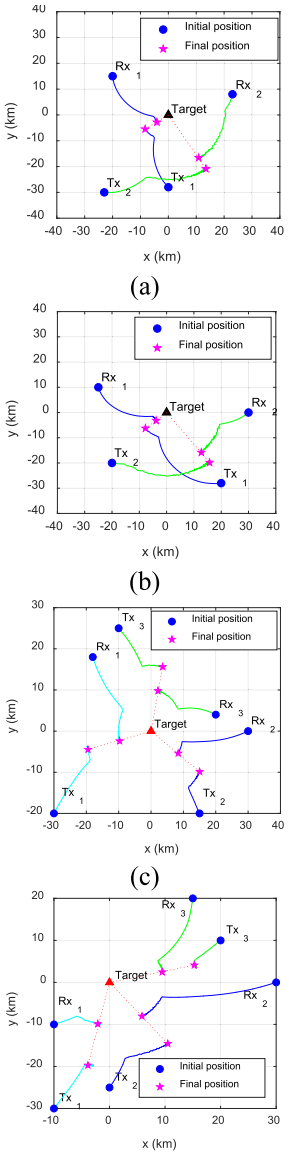

FIGURE 6. Optimal trajectories of UAVs for target localization. (a) 2 × 2 Case I; (b) 2 × 2 Case II; (c) 3 × 3 Case I; (d) 3 × 3 Case II.

It is worth mentioning that the results in (20) and (21) are the same as the ones derived by the authors of [103] in their earlier publication [104] (see (27) and (31a)-(31b) in [104]), where the problem of emitter localization with angle-of-arrival (AOA) sensors carried by the UAVs is considered (note: a factor of 2 is missing since $\beta_i \triangleq 2\theta_i$ is assumed in [104], where θ_i is the angle-of-arrival location of the emitter). It is actually intriguing since locating an emitter transmitting high-power signals actively should be much easier than locating a target passively reflecting signals transmitted by the radar TXs. Moreover, the mechanisms of the two tasks are very different. For example, target localization with bistatic radar involves the concept of the bistatic radar cross section (RCS), which is dependent upon many factors such as the size/shape/material of the target and the bistatic geometry, while emitter localization has nothing to do with the RCS. Also, the radar RXs would have known the waveforms transmitted by the TXs *a priori* (the waveforms transmitted from different TXs could either be same or different), while the AOA sensors wouldn't have access to such knowledge regarding the emitter to be located. Nevertheless, we think both [103] and [104] are great works on UAV path optimization.

3) TARGET VELOCITY ESTIMATION

In [114], the CRLB for target velocity estimation accuracy is derived for DMR consisting of widely separated transmit and receiver antennas, and the problem of antenna deployment optimization based on the CRLB is considered. It is shown that when target is a point scatterer and all antennas are located at similar distances from the target, symmetrically placing the transmit and receive antennas leads to the best velocity estimation performance. Simulation results also show that wider sensor separations lead to better performance in the sense of CRLB of the velocity estimation error.

III. INTERFERENCE SUPPRESSION AND RECEIVER PLACEMENT FOR PRN

A. INTERFERENCE SUPPRESSION

The PRN could be implemented either with or without RC. For PRN with RC, target detection is carried out based on the cross-ambiguity function (CAF) between the direct-path signal collected by the reference channel (RC) and the echo signal collected by the surveillance channel (SC) [36], [37], [43], [44]. For PRN without RC, the inter-channel correlations between the signals collected by the widely separated receivers are exploited for target detection [45]–[49]. It has been reported in [43] that PRN with RC provides better target detection performance than its RC-free counterpart as long as the direct-path reference signal is of acceptable quality. The research works published in the open literatures on PMR without RC could be divided into three subgroups based on the IO waveform model: unknown deterministic processes with i.i.d. temporal samples [45], [46], stochastic processes with temporally-correlated samples [47]–[49], and realistic signal model

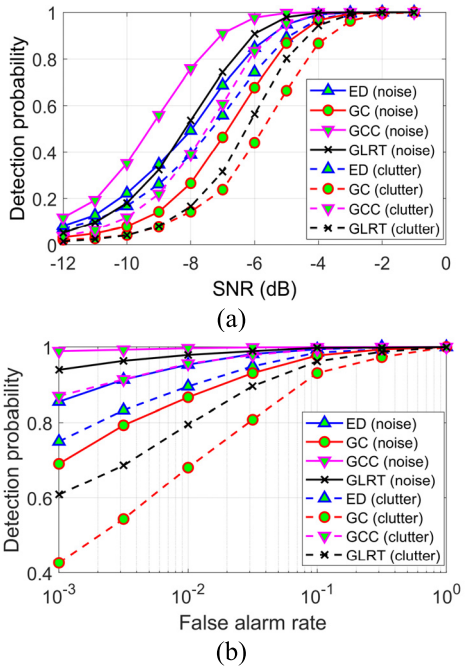

FIGURE 7. Performance degradation of the existing detectors designed for PRN in the presence of unaddressed multipath clutter: (a) $P_{fa} = 0.01$ (b) SNR $= -5$ dB. The solid lines and the dashed lines represent the detection probability of the detectors in the noise-only case and the noise-plus-clutter case, respectively.

depending on the type of IO under consideration [36], [37]. Although it is well-known that the performance of the PRN is under the joint influence of the multi-path clutter, the direct-path interference, the interfering targets, as well as the noise in the received signal, most research works published in the open literatures on the PRN failed to take all of them into consideration.

As an illustrating example, the detection probabilities of the ED detector proposed in [115], the GC detector proposed in [116], the GCC detector proposed in [45], and the GLRT detector proposed in [46] in the noise-only case are plotted in FIGURE 7 (a) and (b) in solid lines assuming $P_{fa} = 0.01$ and SNR $= -5$ dB, respectively. A PMR consists of eight RXs ($N = 8$) and one IO ($M = 1$) is considered, and the signal transmitted from the IO is sampled from $CN(\mathbf{0}, \mathbf{I})$, where CN represents circularly symmetric, complex Gaussian distribution. The number of pulses is assumed to be 30 ($L_p = 30$). The results in FIGURE 7 (a) match perfectly with Fig. 6 (b) in [46]. To show the impact of multi-path clutter on the performance of these detectors, the detection probabilities of these detectors in the presence of light clutter with clutter-to-noise ratio (CNR) of 15 dB are plotted in dashed lines in FIGURE 8 (a) and (b). By comparing the two sets of lines, it is easy to observe that all the detectors suffer noticeable performance degradation in the presence of clutter. Among these detectors, the GC detector [116] and the GLRT detector [46], which are derived assuming unknown noise power, exhibit worse performance than the ED [115] and the GCC [45]. It is worth

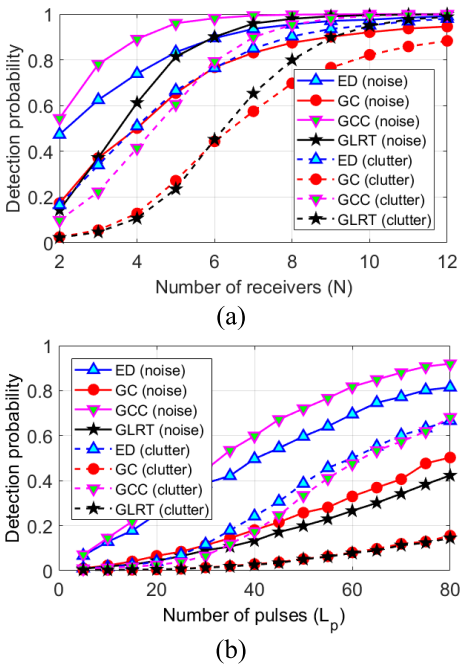

FIGURE 8. Performance degradation of the existing detectors designed for PRN in the presence of unaddressed multipath clutter for different (a) N and (b) L_p. The solid lines and the dashed lines represent the detection probability of the detectors in the noise-only case and the noise-plus-clutter case, respectively.

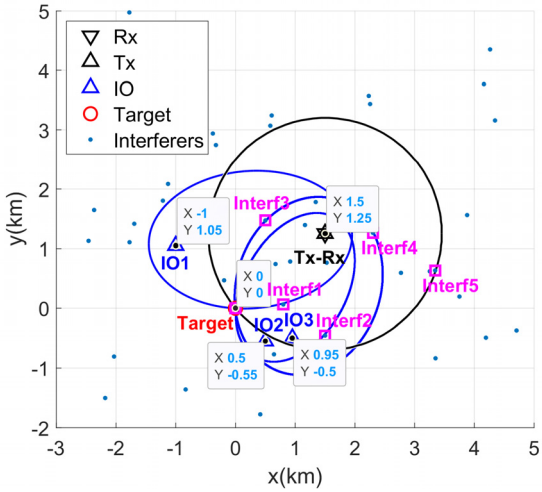

FIGURE 9. Interferences affecting the detection performance of a simple APRN consisting of a co-located MIMO radar and three IOs. The blue dots are randomly generated interferers. The detection performances of the APRN are only affected by the interferers that fell on the same iso-range ellipses (i.e. Interf1-Interf4) and the iso-range circle (i.e. interf5) with the target.

mentioning that although the performance degradation due to the presence of light clutter could be partially compensated by increasing N and L_p, the cost is high. To illustrate the point, the detection probabilities of these detectors for different N given $L_p = 30$ in the noise-only scenario and the noise-plus-clutter (CNR = 15 dB) scenario are plotted in FIGURE 8 (a) in solid and dashed lines, respectively ($P_{fa} = 0.01$, SNR $= -5$ dB). The solid lines match perfectly with Fig. 5 in [46]. It could be seen that although the clutter is light, at least 9 RXs are needed to compensate for the performance loss due to the presence of clutter. And it is reasonable to expect that more RXs are needed if the clutter is heavy. The detection probabilities of these detectors for different L_p given $N = 2$ are plotted in FIGURE 8 (b). It is obvious that increasing L_p doesn't help much in improving the performance of these detectors in the noise-plus-clutter scenario.

B. RECEIVER PLACEMENT

There are two major differences between the antenna placement problems in DMR and PRN. First, since the PRN exploits the illumination from the IOs that already exist, only the positions of the RXs could be optimized by the radar engineers. Second, the positions of the IOs are usually not regularly distributed, hence the symmetric TX-RX geometries that are widely studied for DMR (see Sec. II-B for details) can't be used for PRN. Metrics selected in open literatures as the criterion for optimum receiver placement include the detection probability [106], [117], the SNR [118], [119], the false alarm rate [120], and the transmit power [108], which reflect radar's detection performance. To the authors' best knowledge, the research regarding receiver placement in PRN for improved target measurements is very limited since the accuracy of target localization and velocity estimation is mainly limited by the waveform properties of the signals transmitted from the IOs.

IV. INTERFERENCE SUPPRESSION AND SENSOR GEOMETRY OPTIMIZATION FOR APRN

A. INTERFERENCE SUPPRESSION

The APRN is defined here as a radar system that exploits both the dedicated radar transmit waveforms and signals from other radio-radiation sources. In [53], an APRN network consisting of a monostatic coherent MIMO radar and several IOs was proposed, where the active TX, the active receive array (ARA) and the passive receive array (PRA) are assumed to be co-located. The detection scene considered in [53] is regenerated in FIGURE 9. The interference signals are represented by the blue dots, which are randomly distributed in the area. To determine whether the interference is on the j-th isorange, the bistatic range of the interference is compared with that of the target [20], [53]. The four interference signals on the passive ellipses are marked as Interf1, Interf2, Interf3, and Interf4, respectively, and the interference signal on the active circle is marked as Interf5. To give more flexibility to the sensor geometry, we consider the scenario that multiple active TXs, multiple RXs and multiple IOs are widely separated, and each RX of the APRN consists of two parts: ARA to collect echoes due to the probing signals from the active radar transmitter, and PRA to collect echoes due to the illumination of the IO signals. Each active TX and each IO are assumed to operate at different frequencies, so that the echoes corresponding to different transmit facilities could be separated at the receiving end. Assume that N RXs are

available, the signals received by the ARAs of all the N RXs are combined together before decision making. To suppress the interference in the signals received by the ARAs, the TPCC detector introduced in Section II-A is used if the interference power follows a specific pdf that is known *a priori*, while the GKA detector is used if such information is not available. Similarly, centralized data fusion is performed for the signals received by the PRAs of all the N RXs. And detector could be developed within the GLRT frame to suppress the interference in the signals received by the PRA. The final decision regarding the presence of the target is made by jointly considering the decisions made according to the signals received by the ARAs and the PRAs.

B. SENSOR GEOMETRY OPTIMIZATION

Assume that the positions of the IOs are known *a priori* and fixed, we consider two scenarios in the following: 1) the positions of the ground-based radar TXs/RXs are to be optimized for target detection and localization; and 2) the trajectories of the TXs/RXs mounted on the UAVs are to be planned for target tracking.

1) GEOMETRY OPTIMIZATION FOR GROUND-BASED STATIONARY SENSORS

Although sensor geometry optimization has been intensively studied for DMR [105]–[113] and PRN [117]–[120], similar research is yet to be conducted for APRN, which may be considered as the combination of DMR and PRN. Like PRN, the positions of the IOs in APRN are usually fixed. At the same time, both the positions of the TXs and the RXs could be optimized for improved target detection and localization performance, which is similar to DMR. Considering that the transmit power and the waveforms from the IOs and the TXs are completely different, the problem of sensor optimization of APRN is expected to be much more difficult to solve. Nevertheless, since the APRN provides better performance than the PRN thanks to the additional dedicated radar TXs while costs less than the DMR by using the pre-existing transmitter infrastructure (not to mention it also allows the radar to use the vast low-frequency bands designated for communications systems to monitor the surveillance area continuously without extra power consumption), it has the potential to become a widely-recognized radar network configuration in the near future, hence the reward for addressing this challenging problem is high.

2) PATH PLANNING FOR UAVS EQUIPPED WITH SENSORS

Considering that relative sensor-target geometry significantly affects the performance of target localization performance, using multiple moving sensors with optimized trajectories for target tracking has attracted the attention of many researchers [101], [112], [121], [122]. DMR consisting of single TX at fixed position and multiple RXs carried by UAVs is considered in [112], and the trajectories of the UAVs are optimized by maximizing the determinant of FIM. In [101], target tracking using cognitive radar system composed of multiple radars mounted on UAVs is considered, and the expected cross-entropy is used as the objective function. Three key techniques are incorporated in the proposed cognitive radar system: waveform design, path planning, and sensor selection. However, to the authors' best knowledge, the problem of path planning for UAVs equipped with TXs/RXs given fixed IO positions has not been addressed in the open literature yet.

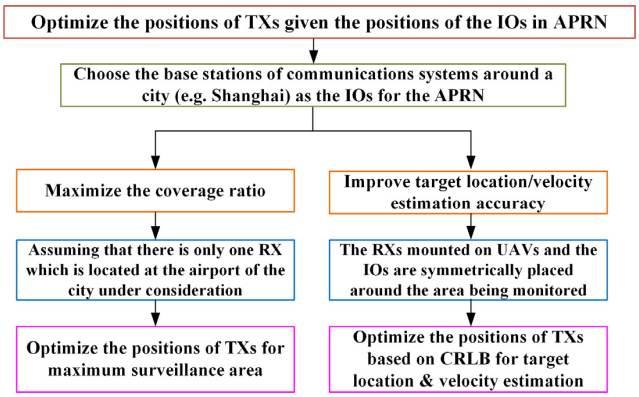

FIGURE 10. Proposed research start-point regarding sensor geometry optimization for APRN: optimize the positions of the TXs given the positions of the IOs in APRN to 1) maximize the surveillance area and 2) improve target location/velocity estimation accuracy.

3) PROPOSED RESEARCH START-POINT REGARDING SENSOR GEOMETRY OPTIMIZATION

Since the problem of sensor geometry optimization for APRN has not been intensively studied yet, we propose a research start-point regarding this problem, which is illustrated in the flowchart in FIGURE 10. We first select some base stations of communications systems around a specific city as the IOs for the APRN, and then we optimize the positions of the active TXs for two typical scenarios. *Scenario I*: assuming that there is only one RX located at the city airport, optimize the positions of a couple of TXs to maximize the surveillance area. *Scenario II*: assuming that several RXs mounted on UAVs and the IOs are symmetrically placed around the area being monitored, optimize the positions of a few TXs based on the CRLB for target location and velocity estimation.

V. MULTISTATIC SAR AND MIMO SAR

A. MULTISTATIC SAR

Monostatic high-resolution SAR system has limited acquisition capability. For example, the TerraSAR-X could map only 2% of the earth's landmass during its 11 days repeat cycle [67]. One possible approach to increasing the mapping rate is to use multiple transmitters/receivers. W. Keydel from the German Aerospace Center predicted the emergence of a software-based multistatic SAR system characterized by multipolarization/multifrequency and a "sensor web" composed of both orbital and terrestrial, fixed and mobile sensing platforms in his famous work—"perspectives and visions for future SAR systems" in 2003. Multistatic SAR could be classified as fully active and semi-active system [68].

In fully active system, multiple sensors are employed and each sensor has both transmit and receive capabilities, for example, the multistatic TechSat 21 flight experiment introduced in [69]. The TechSat 21 flight experiment consisting of three microsatellites, which fly in formation to operate as a virtual large satellite. Each microsatellite RF payload transmits distinguishable signals receives both its own echo and the echoes from the other two satellite RF payloads. The TechSat 21 could be regarded as the earliest ''MIMO SAR'' although the authors didn't use this term. More information about MIMO SAR is to be provided in Sec. V-B.

In semi-active system, only one sensor is transmitting, and multiple widely distributed sensors are employed to receive the echoes from different angles. A good example of semi-active system is the interferometric cartwheel [70], which features three small receiver satellites rotating around each other accompanying the large transmitting master satellite (illuminator). In [123], the performance of three semi-active parasitic InSAR configurations, interferometric cartwheel, cross-track pendulum, and CarPre (a combination of the cartwheel & the pendulum), are evaluated and compared.

Fully active multistatic SAR has higher sensitivity and flexibility at the price of higher cost and computational complexity. Compared with fully active system, the semi-active system is more cost-effective but is more prone to ambiguities. In [68], various spaceborne multistatic SAR configurations are introduced and their strengths and drawbacks for different applications, such as frequent monitoring, cross-track interferometry, and wide-swath imaging, are compared. Specifically, for frequent monitoring problems such as sea ice monitoring, multistatic SAR with a geostationary illuminator and multistatic passive receivers could be used to shorten the revisit time dramatically and provide up-to-data SAR data at a relatively low cost. For example, the revisit time for the European continent could be reduced from serval days to below 1 hour by using 30 small receiver satellites [68]. Some major challenges in implementing multistatic SAR, e.g. phase/time synchronization, are also addressed in [68].

B. MIMO SAR

MIMO SAR system employs multiple sensors that are simultaneously transmitting and receiving. By exploiting the orthogonality between transmit waveforms, each receiving sensor is able to distinguish the echoes associated with different transmit waveforms. According to [127], the first suggestion of using a MIMO SAR architecture emerged in May 2006 in [75], where the concept of multidimensional waveform encoding for spaceborne SAR is introduced. Although the SAR architecture presented in [75], [124], [125] is a typical example of ''MIMO SAR'', Krieger *et al.* only started using this term later in 2008 in their most famous work — [126]. And the term ''MIMO SAR'' actually first appeared in 2007 in [71]–[74].

In [71], the performance of single-input single-output (SISO) SAR, multiple-input single-output (MISO) SAR, phased-array SAR and MIMO SAR ae compared. It is shown that 1) MIMO SAR has the lowest probability of misdetection and highest information gain; 2) MIMO SAR offers higher detector SNR gain when the SNR of the input signal is greater than 0 dB. In [73], the space-time block code (STBC) technique is used for MIMO InSAR. Specifically, the up-chirp and down-chirp LFM signals are used as orthogonal transmit signals and the Alamouti decoder is employed to estimate the geometric information the target. There are several problems regarding the LFM chirp signals used in [73]. First, the simple up-chirp/down-chirp waveform only allows two simultaneous transmissions in the MIMO SAR system. Moreover, according to [127], although the LFM up-chirp and down-chirp are frequently used as transmit waveforms for MIMO radar, they don't actually satisfy the orthogonality condition in a strict sense. In addition, if the width of the scene exceeds the length of the chirps, a significant image quality degradation is expected [127].

Considering that the orthogonality between transmit waveforms plays a significant role in the performance of MIMO SAR, transmit waveform design for MIMO SAR has attracted the attention of many researchers. In [72], a cyclic optimization algorithm is proposed to synthesize constant-modulus transmit signals with good autocorrelation and cross-correlation properties. In [128], [129], the OFDM chirp diverse waveform is designed, which consists of multiple subcarriers and temporal chips (i.e. subpulses). To minimize the interferences between subcarriers, the frequency separation between adjacent subcarriers is carefully designed. Although the OFDM chirp diverse waveform allows for the simultaneous transmission of multiple orthogonal waveforms, it is shown in [127] that when a narrow scene is to be imaged, a periodic pattern (i.e. interference) appears outside the scene since the subpulses of the OFDM chirp diverse waveform are with partially overlapping spectra. To encounter this problem, the short-term shift-orthogonal waveforms are introduced in [67], [126], [127], which are designed to be mutually orthogonal within the time interval that couldn't be resolved by spatial beamforming on receive in elevation.

MIMO SAR could be classified as coherent MIMO SAR and distributed MIMO SAR.

1) COHERENT MIMO SAR

The ARTINO (Airborne Radar for Three-dimensional Imaging and Nadir Observation) system proposed in [74], [76], [130]–[132] is a typical example of coherent MIMO SAR. ARINO is integrated in a small, dismountable UAV and is capable of imaging the direct overflown scene in 3D. It employs a sparse antenna array with M receive antennas widely distributed along the wings and $N/2$ transmit antennas closely located at the tip of each wing. When the transmit antenna spacing is d, which is usually equal to half of the wavelength, the receive antenna spacing is set as $Nd/2$. As a result, a virtual antenna array is formed with each virtual element located at the mean position of each physical

transmit-receive antenna pair. Two methods to separating echo signals associated with different transmit antennas are introduced in [76]: 1) switching, i.e. the transmit antennas are switched from pulse to pulse and only transmit antenna is active at a specific time; 2) frequency diversity, i.e. employ orthogonal transmit waveforms so that all the transmit antennas could transmit simultaneously.

2) DISTRIBUTED MIMO SAR

Compared with coherent MIMO SAR, the major advantages of distributed MIMO SAR include increased spatial coverage, finer geometric resolution, improved ambiguity suppression capabilities, and additional baseline diversity. However, the successful implementation of distributed MIMO SAR demands accurate phase synchronization, which is difficult to maintain in practice for multiple airborne platforms. A typical example of distributed MIMO SAR system is introduced in [77], where multiple widely separated transmit/receive platforms are employed. By exploiting both the monostatic and the bistatic acquisitions, the range resolution improvement factor provided by the proposed MIMO SAR configuration is shown to be much greater than the number of active SAR sensors.

VI. CONCLUSION

With the recent development in high-speed digital processing and time/phase synchronization techniques, sophisticated netted radar systems with high level of integration and centralized data fusion become technically feasible, which include the DMR, the PRN, the APRN, and the MIMO SAR. To fully realize the potentials of these advanced radar networks, three major challenges are identified in this work: interference suppression, adaptive waveform design, and sensor geometry optimization. For DMR, a brief literature review regarding the effective interference suppression approaches presented in the open literature is provided, with the advantages and drawbacks of each method highlighted. Two KA detectors are introduced for target detection in heterogeneous interference and partially homogeneous interference, respectively, which exhibit better performance than the existing detectors. Moreover, adaptive transmit waveform selection for high-speed highly-maneuvering target tracking with DMR is considered. The antenna placement strategies along with the UVA path planning methods for DMR used in the existing research works to realize different optimization goals are also summarized and compared. For PRN, the performance degradation of the existing detectors due to the unaddressed multipath clutter is analyzed. Moreover, the problem of receiver placement in PRN given fixed positions of IOs is investigated. For APRN, the sensor geometry optimization approaches and the path planning strategies with stationary and moving platforms are discussed for the first-time. Considering that imaging is a distinctive function of radar, the key technologies and challenges for implementing multistatic SAR and MIMO SAR are summarized. We believe that this work could serve as a good reference for future researchers interested in developing netted radar systems with widely separated sensors.

ACKNOWLEDGMENTS

The author would like to thank the anonymous reviewers for their insightful comments and suggestions, which definitely made the work more technically sound.

REFERENCES

[1] V. Chernyak, "Multisite radar systems composed of MIMO radars," *IEEE Aerosp. Electron. Syst. Mag.*, vol. 29, no. 12, pp. 28–37, Dec. 2014.
[2] H. Griffiths, "Multistatic, "MIMO and networked radar: The future of radar sensors?" in *Proc. 7th Eur. Radar Conf.*, Paris, France, 2010, pp. 81–84.
[3] H. Griffiths, "Developments in bistatic and networked radar," in *Proc. IEEE CIE Int. Conf. Radar*, Chengdu, China, Oct. 2011, pp. 10–13.
[4] M. I. Mirkin, C. E. Schwartz, and S. Spoerri, "Automated tracking with netted ground surveillance radars," in *Proc. IEEE Int. Radar Conf.*, Washington, DC, USA, Jan. 1980, pp. 371–379.
[5] T. D. Crum, R. E. Saffle, and J. W. Wilson, "An update on the NEXRAD program and future WSR-88D support to operations," *Weather Forecasting*, vol. 13, no. 2, pp. 253–262, Jun. 1998.
[6] M. Malanowski and K. Kulpa, "Two methods for target localization in multistatic passive radar," *IEEE Trans. Aerosp. Electron. Syst.*, vol. 48, no. 1, pp. 572–580, Jan. 2012.
[7] V. Chernyak, *Fundamentals of Multisite Radar Systems*. Boca Raton, FL, USA: CRC Press, Sep. 1998.
[8] J. M. Kurdzo, R. D. Palmer, B. L. Cheong, and M. E. Weber, "Adaptive waveform design for multi-sector array isolation," in *Proc. Eur. Radar Conf. (EuRAD)*, Sep. 2015, pp. 93–96.
[9] A. E. Breiholz, K. M. Kronfeld, K. L. Walling, and R. J. McCabe, "Weather radar system and method with fusion of multiple weather information sources," U.S. Patent 9 535 158 B1, Jan. 3, 2017.
[10] A. E. Breiholz, K. M. Kronfeld, and V. A. Sishtla, "Enhancement of airborne weather radar performance using external weather data," U.S. Patent 9 869 766 B1, Jan. 16, 2018.
[11] S. Guruamy, M. Gadicherla, B. Jayasenthilnathan, and R. W. Burgin, "Methods and systems for providing live weather data onboard an aircraft," U.S. Patent 10 139 474 B2, Nov. 27, 2018.
[12] Z. Li, Y. Zhang, S. Wang, L. Li, and M. Mclinden, "Fast adaptive pulse compression based on matched filter outputs," *IEEE Trans. Aerosp. Electron. Syst.*, vol. 51, no. 1, pp. 548–564, Jan. 2015.
[13] R. Nepal, Y. R. Zhang, G. Zhang, A. Ryzhkov, and W. Blake, "Data quality analysis and enhancement of an airborne weather radar for scientific and multi-mission operations," *Proc. SPIE*, vol. 10633, May 2018, Art. no. 1063308.
[14] J. M. Kurdzo, J. Y. N. Cho, B. L. Cheong, and R. D. Palmer, "A neural network approach for waveform generation and selection with multi-mission radar," in *Proc. IEEE Radar Conf. (RadarConf)*, Apr. 2019, pp. 1–6.
[15] H. Deng, "Orthogonal netted radar systems," *IEEE Aerosp. Electron. Syst. Mag.*, vol. 27, no. 5, pp. 28–35, May 2012.
[16] E. Fishler, A. Haimovich, R. Blum, D. Chizhik, L. Cimini, and R. Valenzuela, "MIMO radar: An idea whose time has come," in *Proc. IEEE Radar Conf.*, Apr. 2004, pp. 71–78.
[17] E. Fishler, A. Haimovich, R. Blum, L. Cimini, D. Chizhik, and R. Valenzuela, "Performance of MIMO radar systems: Advantages of angular diversity," in *Proc. Conf. Rec. 38th Asilomar Conf. Signals, Syst. Comput.*, 2004, pp. 305–309.
[18] E. Fishler, A. Haimovich, R. S. Blum, L. J. Cimini, D. Chizhik, and R. A. Valenzuela, "Spatial diversity in radars-models and detection performance," *IEEE Trans. Signal Process.*, vol. 54, no. 3, pp. 823–838, Mar. 2006.
[19] P. Wang, H. Li, and B. Himed, "Moving target detection using distributed MIMO radar in clutter with nonhomogeneous power," *IEEE Trans. Signal Process.*, vol. 59, no. 10, pp. 4809–4820, Oct. 2011.
[20] H. Li, Z. Wang, J. Liu, and B. Himed, "Moving target detection in distributed MIMO radar on moving platforms," *IEEE J. Sel. Topics Signal Process.*, vol. 9, no. 8, pp. 1524–1535, Dec. 2015.
[21] H. Godrich, A. M. Haimovich, and R. S. Blum, "Target localization accuracy gain in MIMO radar-based systems," *IEEE Trans. Inf. Theory*, vol. 56, no. 6, pp. 2783–2803, Jun. 2010.

[22] A. Haimovich, R. Blum, and L. Cimini, "MIMO radar with widely separated antennas," *IEEE Signal Process. Mag.*, vol. 25, no. 1, pp. 116–129, Jan. 2008.
[23] Q. He, N. H. Lehmann, R. S. Blum, and A. M. Haimovich, "MIMO radar moving target detection in homogeneous clutter," *IEEE Trans. Aerosp. Electron. Syst.*, vol. 46, no. 3, pp. 1290–1301, Jul. 2010.
[24] Y. Lu, C. Han, Z. He, S. Liu, and Y. Wang, "Adaptive JSPA in distributed colocated MIMO radar network for multiple targets tracking," *IET Radar, Sonar Navigat.*, vol. 13, no. 3, pp. 410–419, Mar. 2019.
[25] K. L. Bell, J. T. Johnson, C. J. Baker, G. E. Smith, and M. Rangaswamy, "Modeling and simulation for multistatic coherent MIMO radar," in *Proc. IEEE Radar Conf. (RadarCon)*, Ottawa, ON, Canada, Apr. 2013, pp. 1–6.
[26] T. R. Qureshi, M. Rangaswamy, and K. L. Bell, "Parametric adaptive matched filter for multistatic MIMO radar," *IEEE Trans. Aerosp. Electron. Syst.*, vol. 54, no. 5, pp. 2202–2219, Oct. 2018.
[27] P. Chen, L. Zheng, X. Wang, H. Li, and L. Wu, "Moving target detection using colocated MIMO radar on multiple distributed moving platforms," *IEEE Trans. Signal Process.*, vol. 65, no. 17, pp. 4670–4683, Sep. 2017.
[28] A. Zaimbashi, M. Derakhtian, and A. Sheikhi, "Invariant target detection in multiband FM-based passive bistatic radar," *IEEE Trans. Aerosp. Electron. Syst.*, vol. 50, no. 1, pp. 720–736, Jan. 2014.
[29] A. Zaimbashi, "Broadband target detection algorithm in FM-based passive bistatic radar systems," *IET Radar, Sonar Navigat.*, vol. 10, no. 8, pp. 1485–1499, Oct. 2016.
[30] A. Zaimbashi, "Target detection in analog terrestrial TV-based passive radar sensor: Joint delay-Doppler estimation," *IEEE Sensors J.*, vol. 17, no. 17, pp. 5569–5580, Sep. 2017.
[31] F. Colone, P. Falcone, C. Bongioanni, and P. Lombardo, "WiFi-based passive bistatic radar: Data processing schemes and experimental results," *IEEE Trans. Aerosp. Electron. Syst.*, vol. 48, no. 2, pp. 1061–1079, Apr. 2012.
[32] F. Colone, T. Martelli, C. Bongioanni, D. Pastina, and P. Lombardo, "WiFi-based PCL for monitoring private airfields," *IEEE Aerosp. Electron. Syst. Mag.*, vol. 32, no. 2, pp. 22–29, Feb. 2017.
[33] M. Edrich, F. Meyer, and A. Schroeder, "Design and performance evaluation of a mature FM/DAB/DVB-T multi-illuminator passive radar system," *IET Radar, Sonar Navigat.*, vol. 8, no. 2, pp. 114–122, Feb. 2014.
[34] A. Evers and J. A. Jackson, "Cross-ambiguity characterization of communication waveform features for passive radar," *IEEE Trans. Aerosp. Electron. Syst.*, vol. 51, no. 4, pp. 3440–3455, Oct. 2015.
[35] J. E. Palmer, H. A. Harms, S. J. Searle, and L. Davis, "DVB-T passive radar signal processing," *IEEE Trans. Signal Process.*, vol. 61, no. 8, pp. 2116–2126, Apr. 2013.
[36] S. Gogineni, M. Rangaswamy, B. D. Rigling, and A. Nehorai, "Ambiguity function analysis for UMTS-based passive multistatic radar," *IEEE Trans. Signal Process.*, vol. 62, no. 11, pp. 2945–2957, 2014.
[37] S. Gogineni, M. Rangaswamy, B. D. Rigling, and A. Nehorai, "Cramér–Rao bounds for UMTS-based passive multistatic radar," *IEEE Trans. Signal Process.*, vol. 62, no. 1, pp. 95–106, Jan. 2014.
[38] F. Pieralice, D. Pastina, F. Santi, and M. Bucciarelli, "Multi-transmitter ship target detection technique with GNSS-based passive radar," in *Proc. Int. Conf. Radar Syst. (Radar)*, Oct. 2017, pp. 1–6.
[39] S. Brisken, M. Moscadelli, V. Seidel, and C. Schwark, "Passive radar imaging using DVB-S2," in *Proc. IEEE Radar Conf. (RadarConf)*, May 2017, pp. 552–556.
[40] V. Navratil, J. L. Garry, A. O'Brien, and G. E. Smith, "Utilization of terrestrial navigation signals for passive radar," in *Proc. IEEE Radar Conf. (RadarConf)*, May 2017, pp. 825–829.
[41] V. Navrátil, J. L. Garry, A. J. O'Brien, and G. E. Smith, "Exploiting terrestrial positioning signals to enable a low-cost passive radar," *IEEE Trans. Aerosp. Electron. Syst.*, vol. 54, no. 5, pp. 2246–2256, Oct. 2018.
[42] A. Zaimbashi, M. Derakhtian, and A. Sheikhi, "GLRT-based CFAR detection in passive bistatic radar," *IEEE Trans. Aerosp. Electron. Syst.*, vol. 49, no. 1, pp. 134–159, Jan. 2013.
[43] D. E. Hack, L. K. Patton, B. Himed, and M. A. Saville, "Detection in passive MIMO radar networks," *IEEE Trans. Signal Process.*, vol. 62, no. 11, pp. 2999–3012, Jun. 2014.
[44] X. Zhang, H. Li, J. Liu, and B. Himed, "Joint delay and Doppler estimation for passive sensing with direct-path interference," *IEEE Trans. Signal Process.*, vol. 64, no. 3, pp. 630–640, Feb. 2016.
[45] D. E. Hack, L. K. Patton, B. Himed, and M. A. Saville, "Centralized passive MIMO radar detection without direct-path reference signals," *IEEE Trans. Signal Process.*, vol. 62, no. 11, pp. 3013–3023, Jun. 2014.
[46] J. Liu, H. Li, and B. Himed, "Two target detection algorithms for passive multistatic radar," *IEEE Trans. Signal Process.*, vol. 62, no. 22, pp. 5930–5939, Nov. 2014.
[47] X. Zhang, H. Li, and B. Himed, "A direct-path interference resistant passive detector," *IEEE Signal Process. Lett.*, vol. 24, no. 6, pp. 818–822, Jun. 2017.
[48] X. Zhang, H. Li, and B. Himed, "Multistatic detection for passive radar with direct-path interference," *IEEE Trans. Aerosp. Electron. Syst.*, vol. 53, no. 2, pp. 915–925, Apr. 2017.
[49] X. Zhang, H. Li, and B. Himed, "Multistatic passive detection with parametric modeling of the IO waveform," *Signal Process.*, vol. 141, pp. 187–198, Dec. 2017.
[50] D. W. O'Hagan, M. Ummenhofer, H. Kuschel, and J. Heckenbach, "A passive/active dual mode radar concept," in *Proc. 14th Int. Radar Symp. (IRS)*, vol. 1, Jun. 2013, pp. 136–142.
[51] I. M. Ivashko, O. A. Krasnov, and A. G. Yarovoy, "Receivers topology optimization of the combined active and WiFi-based passive radar network," in *Proc. 11th Eur. Radar Conf.*, Oct. 2014, pp. 517–520.
[52] T. Martelli, C. Bongioanni, F. Colone, P. Lombardo, L. Testa, and A. Meta, "Security enhancement in small private airports through active and passive radar sensors," in *Proc. 17th Int. Radar Symp. (IRS)*, May 2016, pp. 1–5.
[53] Y. Gao, H. Li, and B. Himed, "Joint transmit and receive beamforming for hybrid active–passive radar," *IEEE Signal Process. Lett.*, vol. 24, no. 6, pp. 779–783, Jun. 2017.
[54] T. Brenner, M. Klein, G. Weiss, and H. Kuschel, "Signals and data fusion in a deployable multiband passive-active radar (DMPAR)," in *Proc. IET Int. Conf. Radar Syst. (Radar)*, Oct. 2012, pp. 1–6.
[55] T. Brenner, L. Lamentowski, and R. Mularzuk, "Enhanced target detection by cueing and threshold management in sensor network with DMPAR processing," in *Proc. 18th Int. Radar Symp. (IRS)*, Jun. 2017, pp. 1–9.
[56] H. Kuschel, J. Heckenbach, and J. Schell, "Deployable multiband passive/active radar for air defense (DMPAR)," *IEEE Aerosp. Electron. Syst. Mag.*, vol. 28, no. 9, pp. 37–45, Sep. 2013.
[57] X.-G. Xia, T. Zhang, and L. Kong, "MIMO OFDM radar IRCI free range reconstruction with sufficient cyclic prefix," *IEEE Trans. Aerosp. Electron. Syst.*, vol. 51, no. 3, pp. 2276–2293, Jul. 2015.
[58] Y. L. Sit, B. Nuss, and T. Zwick, "On mutual interference cancellation in a MIMO OFDM multiuser radar-communication network," *IEEE Trans. Veh. Technol.*, vol. 67, no. 4, pp. 3339–3348, Apr. 2018.
[59] J. G. Metcalf, C. Sahin, S. D. Blunt, and M. Rangaswamy, "Analysis of symbol-design strategies for intrapulse radar-embedded communications," *IEEE Trans. Aerosp. Electron. Syst.*, vol. 51, no. 4, pp. 2914–2931, Oct. 2015.
[60] A. Hassanien, M. G. Amin, Y. D. Zhang, and F. Ahmad, "Dual-function radar-communications: Information embedding using sidelobe control and waveform diversity," *IEEE Trans. Signal Process.*, vol. 64, no. 8, pp. 2168–2181, Apr. 2016.
[61] A. Hassanien, M. G. Amin, Y. D. Zhang, and F. Ahmad, "Signaling strategies for dual-function radar communications: An overview," *IEEE Aerosp. Electron. Syst. Mag.*, vol. 31, no. 10, pp. 36–45, Oct. 2016.
[62] P. M. McCormick, S. D. Blunt, and J. G. Metcalf, "Simultaneous radar and communications emissions from a common aperture, part I: Theory," in *Proc. IEEE Radar Conf. (RadarConf)*, May 2017, pp. 1685–1690.
[63] P. M. McCormick, B. Ravenscroft, S. D. Blunt, A. J. Duly, and J. G. Metcalf, "Simultaneous radar and communication emissions from a common aperture, part II: Experimentation," in *Proc. IEEE Radar Conf. (RadarConf)*, May 2017, pp. 1697–1702.
[64] A. Deligiannis, A. Daniyan, S. Lambotharan, and J. A. Chambers, "Secrecy rate optimizations for MIMO communication radar," *IEEE Trans. Aerosp. Electron. Syst.*, vol. 54, no. 5, pp. 2481–2492, Oct. 2018.
[65] Q. He, Z. Wang, J. Hu, and R. S. Blum, "Performance gains from cooperative MIMO radar and MIMO communication systems," *IEEE Signal Process. Lett.*, vol. 26, no. 1, pp. 194–198, Jan. 2019.
[66] M. A. Richards, *Fundamentals of Radar Signal Processing*, 2nd ed. New York, NY, USA: McGraw-Hill, 2014.
[67] G. Krieger, M. Younis, S. Huber, F. Bordoni, A. Patyuchenko, J. Kim, P. Laskowski, M. Villano, T. Rommel, P. Lopez-Dekker, and A. Moreira, "Digital beamforming and MIMO SAR: Review and new concepts," in *Proc. 9th Eur. Conf. Synthetic Aperture Radar (EUSAR)*, Nuremberg, Germany, 2012, pp. 11–14.

[68] G. Krieger and A. Moreira, "Spaceborne bi- and multistatic SAR: Potential and challenges," *IEE Proc.—Radar, Sonar Navigat.*, vol. 153, no. 3, pp. 184–198, Jun. 2006.
[69] M. Martin, P. Klupar, S. Kilberg, and J. Winter, "TechSat 21 and revolutionizing space missions using microsatellites," in *Proc. 15th Amer. Inst. Aeronaut. Astronaut. Conf. Small Satell.*, Logan, UT, USA, 2001, pp. 1–10.
[70] D. Massonnet, "Capabilities and limitations of the interferometric cartwheel," *IEEE Trans. Geosci. Remote Sens.*, vol. 39, no. 3, pp. 506–520, Mar. 2001.
[71] W. Wang, "Applications of MIMO technique for aerospace remote sensing," in *Proc. IEEE Aerosp. Conf.*, Big Sky, MT, USA, Mar. 2007, pp. 1–10.
[72] J. Li, X. Zheng, and P. Stoica, "MIMO SAR imaging: Signal synthesis and receiver design," in *Proc. 2nd IEEE Int. Workshop Comput. Adv. Multi-Sensor Adapt. Process.*, St. Thomas, VI, USA, Dec. 2007, pp. 89–92.
[73] J.-H. Kim, A. Ossowska, and W. Wiesbeck, "Investigation of MIMO SAR for interferometry," in *Proc. Eur. Radar Conf.*, Munich, Germany, Oct. 2007, pp. 51–54.
[74] J. H. G. Ender, "MIMO-SAR," in *Proc. Int. Radar Symp.*, Cologne, Germany, 2007, pp. 667–674.
[75] G. Krieger, N. Gebert, and A. Moreira, "Digital beamforming techniques for spaceborne radar remote sensing," presented at the Eur. Conf. Synthetic Aperture Radar (EUSAR), Dresden, Germany, 2006.
[76] J. H. G. Ender and J. Klare, "System architectures and algorithms for radar imaging by MIMO-SAR," in *Proc. IEEE Radar Conf.*, Pasadena, CA, USA, May 2009, pp. 1–6.
[77] D. Cristallini, D. Pastina, and P. Lombardo, "Exploiting MIMO SAR potentialities with efficient cross-track constellation configurations for improved range resolution," *IEEE Trans. Geosci. Remote Sens.*, vol. 49, no. 1, pp. 38–52, Jan. 2011.
[78] A. Zaimbashi, "Forward M-ary hypothesis testing based detection approach for passive radar," *IEEE Trans. Signal Process.*, vol. 65, no. 10, pp. 2659–2671, May 2017.
[79] S. M. Kay, *Fundamentals of Statistical Signal Processing: Detection Theory*, vol. 2. Upper Saddle River, NJ, USA: Prentice-Hall, 1998.
[80] S. M. Kay, *Fundamentals of Statistical Signal Processing: Estimation Theory*, vol. 1. Upper Saddle River, NJ, USA: Prentice-Hall, 1993.
[81] C. Yuan Chong, F. Pascal, J.-P. Ovarlez, and M. Lesturgie, "MIMO radar detection in non-Gaussian and heterogeneous clutter," *IEEE J. Sel. Topics Signal Process.*, vol. 4, no. 1, pp. 115–126, Feb. 2010.
[82] P. Wang, H. Li, and B. Himed, "A parametric moving target detector for distributed MIMO radar in non-homogeneous environment," *IEEE Trans. Signal Process.*, vol. 61, no. 9, pp. 2282–2294, May 2013.
[83] Y. Gao, H. Li, and B. Himed, "Knowledge-aided range-spread target detection for distributed MIMO radar in nonhomogeneous environments," *IEEE Trans. Signal Process.*, vol. 65, no. 3, pp. 617–627, Feb. 2017.
[84] J. Liu, H. Li, and B. Himed, "Persymmetric adaptive target detection with distributed MIMO radar," *IEEE Trans. Aerosp. Electron. Syst.*, vol. 51, no. 1, pp. 372–382, Jan. 2015.
[85] B. Shtarkalev and B. Mulgrew, "Multistatic moving target detection in unknown coloured Gaussian interference," *Signal Process.*, vol. 115, pp. 130–143, Oct. 2015.
[86] A. Aubry, A. De Maio, and L. Pallotta, "A geometric approach to covariance matrix estimation and its applications to radar problems," *IEEE Trans. Signal Process.*, vol. 66, no. 4, pp. 907–922, Feb. 2018.
[87] N. Li, H. Yang, G. Cui, L. Kong, and Q. Huo Liu, "Adaptive two-step Bayesian MIMO detectors in compound-Gaussian clutter," *Signal Process.*, vol. 161, pp. 1–13, Aug. 2019.
[88] P. Wang, Z. Wang, H. Li, and B. Himed, "Knowledge-aided parametric adaptive matched filter with automatic combining for covariance estimation," *IEEE Trans. Signal Process.*, vol. 62, no. 18, pp. 4713–4722, Sep. 2014.
[89] A. Aubry, A. De Maio, L. Pallotta, and A. Farina, "Covariance matrix estimation via geometric barycenters and its application to radar training data selection," *IET Radar, Sonar Navigat.*, vol. 7, no. 6, pp. 600–614, Jul. 2013.
[90] J.-H. Won, J. Lim, S.-J. Kim, and B. Rajaratnam, "Condition number regularized covariance estimation," Stanford Univ., Stanford, CA, USA, Tech. Rep. 2012-10, 2012.
[91] A. Aubry, A. De Maio, L. Pallotta, and A. Farina, "Maximum likelihood estimation of a structured covariance matrix with a condition number constraint," *IEEE Trans. Signal Process.*, vol. 60, no. 6, pp. 3004–3021, Jun. 2012.
[92] Z. Shang, X. Li, Y. Liu, Y. Wang, and W. Liu, "GLRT detector based on knowledge aided covariance estimation in compound Gaussian environment," *Signal Process.*, vol. 155, pp. 377–383, Feb. 2019.
[93] E. Jay, J. P. Ovarlez, D. Declercq, and P. Duvaut, "BORD: Bayesian optimum radar detector," *Signal Process.*, vol. 83, no. 6, pp. 1151–1162, Jun. 2003.
[94] K. J. Sangston, F. Gini, and M. S. Greco, "Coherent radar target detection in heavy-tailed compound-Gaussian clutter," *IEEE Trans. Aerosp. Electron. Syst.*, vol. 48, no. 1, pp. 64–77, Jan. 2012.
[95] Y. Zhao, S. Wan, S. Lu, J. Sun, and P. Lei, "Exploiting the persymmetric property of covariance matrices for knowledge-aided space-time adaptive processing," *IEEE Access*, vol. 6, pp. 68001–68012, 2018.
[96] N. Kang, Z. Shang, and Q. Du, "Knowledge-aided structured covariance matrix estimator applied for radar sensor signal detection," *Sensors*, vol. 19, no. 3, p. 664, Feb. 2019.
[97] G. Sun, Z. He, and Y. Zhang, "Distributed airborne MIMO radar detection in compound-Gaussian clutter without training data," *Circuits, Syst., Signal Process.*, vol. 37, no. 10, pp. 4617–4636, Oct. 2018.
[98] D. J. Kershaw and R. J. Evans, "Waveform selective probabilistic data association," *IEEE Trans. Aerosp. Electron. Syst.*, vol. 33, no. 4, pp. 1180–1188, Oct. 1997.
[99] S. P. Sira, A. Papandreou-Suppappola, and D. Morrell, "Dynamic configuration of time-varying waveforms for agile sensing and tracking in clutter," *IEEE Trans. Signal Process.*, vol. 55, no. 7, pp. 3207–3217, Jul. 2007.
[100] S. P. Sira, Y. Li, A. Papandreou-Suppappola, D. Morrell, D. Cochran, and M. Rangaswamy, "Waveform-agile sensing for tracking," *IEEE Signal Process. Mag.*, vol. 26, no. 1, pp. 53–64, Jan. 2009.
[101] Y. Xiang, M. Akcakaya, S. Sen, D. Erdogmus, and A. Nehorai, "Target tracking via recursive Bayesian state estimation in cognitive radar networks," *Signal Process.*, vol. 155, pp. 157–169, Feb. 2019.
[102] N. H. Nguyen, K. Dogancay, and L. M. Davis, "Joint transmitter waveform and receiver path optimization for target tracking by multistatic radar system," in *Proc. IEEE Workshop Stat. Signal Process. (SSP)*, Gold Coast, VIC, Australia, Jun. 2014, pp. 444–447.
[103] N. H. Nguyen and K. Doğançay, *Signal Processing for Multistatic Radar Systems*. New York, NY, USA: Academic, 2020, pp. 13–32 and 99–110.
[104] K. Doğançay and H. Hmam, "Optimal angular sensor separation for AOA localization," *Signal Process.*, vol. 88, no. 5, pp. 1248–1260, May 2008.
[105] Y. Yang, W. Yi, T. Zhang, G. Cui, L. Kong, X. Yang, and J. Yang, "Fast optimal antenna placement for distributed MIMO radar with surveillance performance," *IEEE Signal Process. Lett.*, vol. 22, no. 11, pp. 1955–1959, Nov. 2015.
[106] Y. Yang, W. Yi, T. Zhang, G. Cui, L. Kong, and X. Yang, "Antenna placement of multistatic radar system with detection and localization performance," in *Proc. 19th Int. Conf. Inf. Fusion (FUSION)*, Heidelberg, Germany, Jul. 2016, pp. 620–625.
[107] X. Sun, Y. Yang, W. Yi, and L. Kong, "Fast dynamic deployment of mobile sensor networks for the changing monitoring requirements," in *Proc. IEEE Radar Conf. (RadarConf)*, Seattle, WA, USA, May 2017, pp. 1726–1731.
[108] M. Radmard, M. M. Chitgarha, M. N. Majd, and M. M. Nayebi, "Antenna placement and power allocation optimization in MIMO detection," *IEEE Trans. Aerosp. Electron. Syst.*, vol. 50, no. 2, pp. 1468–1478, Apr. 2014.
[109] Y. Yang, T. Zhang, W. Yi, L. Kong, X. Li, B. Wang, and X. Yang, "Deployment of multistatic radar system using multi-objective particle swarm optimisation," *IET Radar, Sonar Navigat.*, vol. 12, no. 5, pp. 485–493, 2018.
[110] T. Zhang, J. Liang, Y. Yang, G. Cui, L. Kong, and X. Yang, "Antenna deployment method for multistatic radar under the situation of multiple regions for interference," *Signal Process.*, vol. 143, pp. 292–297, Feb. 2018.
[111] H. Godrich, A. P. Petropulu, and H. V. Poor, "Sensor selection in distributed multiple-radar architectures for localization: A knapsack problem formulation," *IEEE Trans. Signal Process.*, vol. 60, no. 1, pp. 247–260, Jan. 2012.
[112] N. H. Nguyen and K. Dogancay, "Optimal geometry analysis for multistatic TOA localization," *IEEE Trans. Signal Process.*, vol. 64, no. 16, pp. 4180–4193, Aug. 2016.

[113] W.-J. Chen and R. M. Narayanan, "Antenna placement for minimizing target localization error in UWB MIMO noise radar," *IEEE Antennas Wireless Propag. Lett.*, vol. 10, pp. 135–138, 2011.
[114] Q. He, R. S. Blum, H. Godrich, and A. M. Haimovich, "Target velocity estimation and antenna placement for MIMO radar with widely separated antennas," *IEEE J. Sel. Topics Signal Process.*, vol. 4, no. 1, pp. 79–100, Feb. 2010.
[115] P. Wang, J. Fang, N. Han, and H. Li, "Multiantenna-assisted spectrum sensing for cognitive radio," *IEEE Trans. Veh. Technol.*, vol. 59, no. 4, pp. 1791–1800, May 2010.
[116] D. Cochran, H. Gish, and D. Sinno, "A geometric approach to multiple-channel signal detection," *IEEE Trans. Signal Process.*, vol. 43, no. 9, pp. 2049–2057, Sep. 1995.
[117] J. Yi, X. Wan, and H. Leung, "Receiver placement in multistatic passive radars," in *Proc. IEEE Radar Conf. (RadarCon)*, Arlington, VA, USA, May 2015, pp. 876–879.
[118] M. Ben Kilani, G. Gagnon, and F. Gagnon, "Multistatic radar placement optimization for cooperative radar-communication systems," *IEEE Commun. Lett.*, vol. 22, no. 8, pp. 1576–1579, Aug. 2018.
[119] M. M. Chitgarha, M. Radmard, M. N. Majd, B. H. Khalaj, and M. M. Nayebi, "The detector's output SNR as a criterion for receiver placement in MIMO DVB-T based passive coherent location," in *Proc. IV Int. Congr. Ultra Modern Telecommun. Control Syst.*, St. Petersburg, Russia, Oct. 2012, pp. 431–435.
[120] M. N. Majd, M. M. Chitgarha, M. Radmard, and M. M. Nayebi, "Probability of missed detection as a criterion for receiver placement in MIMO PCL," in *Proc. IEEE Radar Conf.*, Atlanta, GA, USA, May 2012, pp. 924–927.
[121] K. Zhou and S. I. Roumeliotis, "Optimal motion strategies for range-only constrained multisensor target tracking," *IEEE Trans. Robot.*, vol. 24, no. 5, pp. 1168–1185, Oct. 2008.
[122] F. Morbidi and G. L. Mariottini, "Active target tracking and cooperative localization for teams of aerial vehicles," *IEEE Trans. Control Syst. Technol.*, vol. 21, no. 5, pp. 1694–1707, Sep. 2013.
[123] G. Krieger, H. Fiedler, J. Mittermayer, K. Papathanassiou, and A. Moreira, "Analysis of multistatic configurations for spaceborne SAR interferometry," *IEE Proc.—Radar, Sonar Navigat.*, vol. 150, no. 3, pp. 87–96, Jun. 2003.
[124] G. Krieger, N. Gebert, and A. Moreira, "Multidimensional waveform encoding for synthetic aperture radar remote sensing," in *Proc. IET Int. Conf. Radar Syst.*, Edinburgh, U.K., 2007, pp. 1–5.
[125] G. Krieger, N. Gebert, and A. Moreira, "Multidimensional radar waveforms a new paradigm for the design and operation of highly performant spaceborne synthetic aperture radar systems," in *Proc. IEEE Int. Geosci. Remote Sens. Symp.*, Barcelona, Spain, 2007, pp. 4937–4941.
[126] G. Krieger, N. Gebert, and A. Moreira, "Multidimensional waveform encoding: A new digital beamforming technique for synthetic aperture radar remote sensing," *IEEE Trans. Geosci. Remote Sens.*, vol. 46, no. 1, pp. 31–46, Jan. 2008.
[127] G. Krieger, "MIMO-SAR: Opportunities and pitfalls," *IEEE Trans. Geosci. Remote Sens.*, vol. 52, no. 5, pp. 2628–2645, May 2014.
[128] W.-Q. Wang, "Mitigating range ambiguities in high-PRF SAR with OFDM waveform diversity," *IEEE Geosci. Remote Sens. Lett.*, vol. 10, no. 1, pp. 101–105, Jan. 2013.
[129] W.-Q. Wang, "MIMO SAR OFDM chirp waveform diversity design with random matrix modulation," *IEEE Trans. Geosci. Remote Sens.*, vol. 53, no. 3, pp. 1615–1625, Mar. 2015.
[130] J. Klare, "A new airborne radar for 3D imaging—Simulation study of ARTINO," in *Proc. Eur. Conf. Synthetic Aperture Radar (EUSAR)*, Dresden, Germany, May 2006, pp. 1–4.
[131] J. Klare, M. Weiss, O. Peters, A. Brenner, and J. Ender, "ARTINO: A new high resolution 3D imaging radar system on an autonomous airborne platform," in *Proc. IEEE Int. Symp. Geosci. Remote Sens.*, Denver, CO, USA, Jul. 2006, pp. 3842–3845.
[132] J. Klare, D. Cerutti-Maori, A. Brenner, and J. Ender, "Image quality analysis of the vibrating sparse MIMO antenna array of the airborne 3D imaging radar ARTINO," in *Proc. IEEE Int. Geosci. Remote Sens. Symp.*, Barcelona, Spain, Jul. 2007, pp. 5310–5314.

ZHE GENG (Member, IEEE) received the B.S. degrees *(magna cum laude)* in electrical engineering from Florida International University (FIU), Miami, FL, USA, and the Hebei University of Technology, Tianjin, China, in 2012, and the Ph.D. degree in electrical engineering from FIU in 2018. From 2018 to 2019, she was a Research Scientist with Wright State University, Dayton, OH, USA. In December 2019, she joined the College of Electronic and Information Engineering, Nanjing University of Aeronautics and Astronautics (NUAA), where she is currently an Associate Professor. She was a recipient of FIU's most prestigious awards for entering doctoral students, the FIU Presidential Fellowship. Her research interests include distributed MIMO radar and joint radar-communications systems. She is the 2nd author of *Radar Networks*, which was published by CRC press in June 2020.